Journal Pre-proof

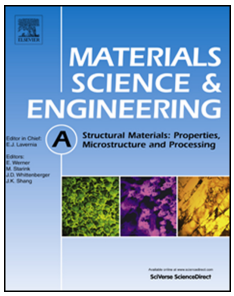

Accounting for the effect of dislocation climb-mediated flow on the anisotropy and texture evolution of Mg alloy, AZ31B

M.A. Ritzo, R.A. Lebensohn, L. Capolungo, S.R. Agnew

PII: S0921-5093(21)01841-4

DOI: https://doi.org/10.1016/j.msea.2021.142581

Reference: MSA 142581

To appear in: *Materials Science & Engineering A*

Received Date: 8 November 2021

Revised Date: 25 December 2021

Accepted Date: 28 December 2021

Please cite this article as: M.A. Ritzo, R.A. Lebensohn, L. Capolungo, S.R. Agnew, Accounting for the effect of dislocation climb-mediated flow on the anisotropy and texture evolution of Mg alloy, AZ31B, *Materials Science & Engineering A* (2022), doi: https://doi.org/10.1016/j.msea.2021.142581.

M.A. Ritzo: Investigation, Writing – original draft, R.H Lebensohn: Software, Writing – review & editing, L. Capolungo: Visualization, Writing – review & editing, S.R. Agnew: Conceptualization, Supervision, Writing – original draft, Writing – review & editing

Accounting for the effect of dislocation climb-mediated flow on the anisotropy and texture evolution of Mg alloy, AZ31B

M.A. Ritzo[a], R.A. Lebensohn[b], L. Capolungo[c], and S.R. Agnew[a,*]

[a]Department of Materials Science and Engineering, University of Virginia, Charlottesville, VA, 22904-4745, USA

[b]Theoretical Division, Los Alamos National Laboratory, Los Alamos, NM, 87544, USA

[c]Material Science and Technology Division, MST-8, Los Alamos National Laboratory, Los Alamos, 87545 NM, USA

*Corresponding Author: address - Department of Materials Science and Engineering, University of Virginia, Charlottesville, VA, 22904, USA
email – agnew@virginia.edu (S.R. Agnew)

Abstract

The current study explores the role that dislocation climb has in mediating plasticity a Mg alloy at moderately elevated temperatures. Interrupted tensile tests were performed on samples of Mg alloy, AZ31B, sheet in the O temper condition over a range of strain rates (10^{-5} to 10^{-1} s^{-1}) and temperatures (20 – 350 $^{\circ}$C) along the rolling and transverse directions. Experimental measurements of the resulting strain anisotropy and texture evolution were used as constraints during a parametric study employing a new crystal plasticity model (VPSC-CLIMB), which explicitly accounts for the kinematics of dislocation climb. The results reveal that the climb of basal <a> dislocations is not only important for dislocation recovery, but also demonstrate that climb accommodates a significant fraction of the strain in conditions where a power-law creep-type constitutive response prevails. This work does not discredit the notion that non-basal slip of <a> and <c+a> dislocations is important over a wide range of temperatures and strain rates. However, it demonstrates that the activation of dislocation climb as the mechanistic change within the power law regime provides an explanation for a wide range of observations, including the simultaneous reduction in strain anisotropy, slowed texture evolution, and rapid increase in strain rate sensitivity. Finally, it is hypothesized that these conclusions may even apply to cases in which grain boundary sliding and/or dynamic recrystallization are observed.

Keywords: dislocation, climb, anisotropy, texture, crystal plasticity

1- Introduction

Many attempts have been made to explain the improved ductility of magnesium alloys at moderately high temperatures (> 100 $^{\circ}$C). They tend to focus *either* on the phenomenological aspects (i.e., increased strain rate sensitivity, lowered flow stress) *or* the possibility of increased activation of non-basal slip mechanisms. There is no doubt that increases in strain rate sensitivity forestall catastrophic plastic instability and thereby increase post uniform elongation [1] and a

lowered flow stress will lower the driving force for fracture. There is also no doubt that non-basal slip mechanisms play a critical role in the deformation of Mg and its alloys, even at low temperatures. The seminal work of Couret & Caillard [2] demonstrated the importance of the cross glide of <a> dislocations into prism and pyramidal planes during tensile deformation. This has implications for the macroscopic deformation as it leads to high r-values and a characteristic texture evolution which aligns the prism planes [3].

Other non-basal slip modes are also thought to play a large role in deformation in order to satisfy the Von Mises criterion, which states that 5 independent slip systems are needed in order to accommodate arbitrary deformation [4]. At room temperature, basal and prism glide alone only account for 4 (2 from basal and 2 from prism) independent slip systems and cannot accommodate straining along the <c> axis. These concerns can be addresssed through the activation of <c+a> slip, which has been linked to the enhanced room temperature ductility of Mg-Li [5,6] and Mg-Y [6,7] alloys. However, <c+a> slip is known to have a higher critical resolved shear stress (CRSS) than basal and prism slip <a> [8], which accounts for its relatively low activity during uniaxial tension in common Mg alloys (e.g., AZ31). The role of <c+a> slip in these alloys has been emphasized under other straining conditions, most notably uniaxial compression [9]. The ease of <c+a> motion was successfully used as a predictor for enhanced ambient temperature ductility of various Mg alloy systems [10]. In that model, failure is seen as a competition between two processess: the dissociation of <c+a> dislocations onto basal planes where they are sessile (the pyramidal to basal transition) and their cross slip between pyramidal planes. It is suggested that ductility of Mg alloys may be increased through alloying by lowering the energetic barrier to <c+a> cross glide.

In addition to its effects on room temperature deformation, the activation of <c+a> glide is viewed as the critical mechanism for high temperature deformation of Mg alloys in the literature for several reasons. First, the density of <c+a> dislocations is observed to increase with increasing deformation temperature [11], which suggests increased slip activity consistent with the knowledge that the CRSS of <c+a> slip is strongly temperature sensitive [8]. From the work of Wu et al. [10], it seems reasonable that increasing the temperature would also enhance the ease of <c+a> slip, since the proposed critical barrier, cross slip, is a thermally activated process. Agnew & Duygulu [3] explored this line of thinking earlier by using <c+a> slip to match the reduced strain anisotropy observed at high temperatures and claimed it could explain the texture evolution. However, their texture data showed that employing sufficient <c+a> glide to explain the low r-value led to a clear splitting of the peaks in basal pole figure intensity toward the tensile axis, which is a direct result of the motion of <c+a> dislocations, since it causes the crystals with c-axes initially close to the normal direction to rotate toward the tensile direction.

In addition, other characteristics of high temperature deformation cannot be explained through <c+a> slip; namely, the strongly increased strain rate sensitivity and the stress-independent activation energy of deformation within the power law regime. The strain rate sensitivity of Mg alloys at ambient temperature (m~0.01-0.02) where the glide of dislocations clearly dominates the deformation [12]. Some alloys are known to exhibit increased strain rate sensitivity despite being glide-controlled creep (i.e., viscous glide), but this is attributed to the solute drag [13],

rather than the activation of additional glide modes. Wu et al.[10] estimate the activation free energy energy of <c+a> cross slip between pyramidal planes in the Mg alloy AZ31B to be ~ 0.55 eV/atom (~53 kJ/mol) [10], which is much lower than the stress-independent activation energies typically found in literature for the power law creep regime (110 kJ/mol [14], 140 kJ/mol [15]). In light of these inconsistencies, it is clear that another mechanism must be at work.

When compared to glide modes, less attention has been given to the role of dislocation climb mechanisms within recent crystal plasticity studies of Mg alloys, even though classical studies of creep deformation noted the importance of dislocation climb in certain temperature and strain rate regimes [16–18]. Incorporation of dislocation climb also has the potential to address the shortcomings of prior studies to adequately account for the texture evolution [19], as will be explained in greater detail later. The activation of significant climb can also address the activation energy and increased rate sensitivity as climb is controlled through the diffusion of vacancies (Q = 92 – 135 kJ/mol, depending on whether the rate-controlling step is along high diffusivity paths such as dislocation cores/grain boundaries or the lattice, respectively) and has been theorized to result in increased strain rate sensitivity [20]. This study tests the hypothesis that the reduced strain accomodation through dislocation glide and increased activation of climb is the cause of the observed slowed texture evolution during high temperature deformation and associated changes in the constitutive response.

There are at least three other mechanisms which may affect the plasticity and texture evolution at high temperatures: grain growth, grain boundary sliding (GBS), and dynamic recrystallization (DRX) [21]. Stress-assisted grain growth has been previously observed in nanocrystalline Cu [22] and Al [23] as a mechanism to reduce the interfacial energy stored in the grain boundaries. Previous studies in AZ31 have shown that grain growth has two major effects on texture: the strengthening of the basal texture [24] and the strengthening of a $< 11\bar{2}0 >$ component due to anomalous grain growth [25]. The existing basal texture from the rolling process tends to be disrupted during GBS [26,27], which was only observed in the texture collected in the GBS regime. Staroselsky and Anand (2003) found it was necessary to use a non crystallographic term representing GBS during their crystal plasticity finite element modeling (CPFEM) of simulate room temperature deformation of HCP Mg [28]. DRX is also a possibility; however, this tends to randomize the texture since the newly recrystallized grains have essentially random orientations [21,29]. Furthermore, a recent study of grain boundary serration (an important mechanism of DRX) has emphasized the role of grain boundary dislocations and grain boundary sliding [30] demonstrating the interconnected nature of all these mechanisms.

Finally, it is noted that climb is not exclusive to dislocations. Disconnections – line defects found on interfaces (including grain boundaries) with a Burgers vector and step height – are believed to glide and climb during processes such as GBS [31]. Some amount of GBS is required to suppress void formation during deformation, whether the bulk deformation is diffusional (Lifshitz GBS) [32] or dislocation-based (Rachinger GBS) [33]. Following the model proposed by Ball and Hutchinson [34], GBS (possibly induced by the motion of grain boundary dislocations and/or disconnections impeded by triple junctions and other obstacles) can itself use a “glide and climb” approach to overcome the obstacles and continue sliding. The process is generally believed to be

rate-controlled by climb and plays a key role in superplasticity. The role of intragranular dislocation motion in temperature and strain rate regimes where GBS is operative is still a matter of debate. Some authors have suggested that a primary role of intragranular dislocation motion is to generate grain boundary dislocations in order to accommodate GBS [35], whereas early work by Ashby & Verrall [36] suggested that GBS and dislocation creep could both contribute to the deformation over a relatively wide range of strain rate. Prior work by the one of the present authors [15] revealed that moderate grain size differences (6 vs 8 μm) between sheets with nearly identical chemistry and texture resulted in higher rate sensitivities (0.27 vs 0.23) for the finer grained material. The difference was abscribed to the activation of GBS in the sample with the smaller grain size in accordance with the findings of Barnett et al [37], placing it on the boundary between high temperature creep and GBS.

The present study employs a combination of mechanical testing, texture measurements by x-ray diffraction, and crystal plasticity modelling using a new version of the viscoplastic self-consistent (VPSC-CLIMB) code that explicitly incorporates the kinematics of dislocation climb to model the response of Mg alloy AZ31B. The goal of the study is to test the hypothesis that the climb of <a> type edge dislocations can explain the transitions in texture evolution and strain anisotropy which are observed to occur in Mg alloy samples deformed at moderately elevated temperatures.

2- Deformation Mechanisms Considered in the Present Study

Gliding dislocations induce simple shear on the glide plane and in the glide direction (parallel to its Burgers vector). Depending upon the boundary conditions to which a crystal is subjected, it will undergo rigid-body rotation, lattice rotation or both. This is the main reason why deformed polycrystals develop preferred orientations (crystallographic texture). Each glide mode has a characteristic impact on the texture and plastic anisotropy, a point which will play a critical role in the present study of the extent to which climb mechanism accommodate strain during high temperature deformation. Out of the several major glide modes known to operate in magnesium in this temperature and strain rate regime, the simulations in this study will rely on three of the most prominent: basal $\{0001\}\langle 11\bar{2}0\rangle$ (the easy slip mode in Mg), prism $\{1\bar{1}00\}\langle 11\bar{2}0\rangle$, and 2nd order pyramidal $\{11\bar{2}\bar{2}\}\langle 11\bar{2}3\rangle$ (<c+a> slip) which has been experimentally observed [8], and used in prior simulations (e.g., [3,38,39]). Pyramidal <a> $\{1\bar{1}00\}\langle 11\bar{2}0\rangle$ slip is also a possibility, however, it cannot be readily discriminated from the concurrent operation of basal and prismatic <a> slip [6].

Deformation twinning on $\{10\bar{1}2\}$ type planes is also an important mechanism in Mg, which is taken into account, though its role is minimized in the present study by the initial sheet texture and in-plane tensile strain paths under consideration. The influence of twinning on the constitutive behavior and texture evolution of Mg is a topic which has been deeply investigated (e.g.,[40–42]).

The most obvious candidate dislocations to consider the role of climb are the prominent basal <a>, $\{0001\}\langle 11\bar{2}0\rangle$, type dislocations due to their ubiquity in Mg alloys. Another possibility is the climb of prism <c>, $\{10\bar{1}0\}\langle 0001\rangle$, dislocations. Typically, <c> dislocations are not

observed to glide and multiply in single crystals because crystals well oriented for this glide mode will deform instead via the softer basal glide mechanism. Previous experimental observations of <c> dislocation climb were made by Stohr & Poirier [43] in their landmark study of <c+a> slip after compressive deformation of c-axis aligned crystals at the highest temperatures. Edelin & Poirier [44] also observed the importance of <c> dislocation climb in <c> compression, at the highest temperatures (T ~ 500 °C). However, the effects of <c> climb are excluded in this study due to their significantly lower densities compared to <a> dislocations. Similar to glide, dislocation climb has unique texture and strain anisotropy characteristics that can be used to discriminate its activity using polycrystal plasticity simulations. The kinematics of crystal plasticity associated with dislocation climb remains an open research question, which is taken up in the present study.

3- Temperature, stress, and strain rate regime of interest

Flow stress – strain rate data from recent studies of [14](solid lines) and [45](dashed lines) are presented to illustrate the regimes in which particular deformation mechanisms dominate (Figure 1). The strain rate sensitivities of the flow stress can aid in the determination of the dominant deformation mechanism: ~0.125 – 0.143 ("low temperature" pipe diffusion-controlled dislocation climb and glide), ~0.2-0.25 ("high temperature" lattice diffusion-controlled dislocation climb and glide), ~0.33 – 0.5 (grain boundary sliding (GBS)), and ~1 (diffusional flow by Coble (grain boundary diffusion) creep). Nabarro-Herring creep is not relevant to the present study, due to the small grain size (< 10 μm) of the examined samples, which favors Coble creep. Employing established constitutive relationships, e.g., from the seminal work of Frost & Ashby [46], activation energies for pipe and lattice diffusion from Antoniswamy et al. [14], the remaining material constants needed to describe high and low temperature creep and GBS of 1.1 x 10^6 and 1.71, respectively, were obtained by performing least-squares regression of all the available data. Thick solid lines in the figure represent the borders of a deformation mechanism map [46] for the material with a grain size of ~5.3 μm [14] and thick dashed lines represent the borders for a material with a grain size of 4.5 μm [45]. Note that the material used by Antoniswamy et al. [14] was tested in the H24 temper, which made initial grain size measurements difficult. The quoted grain size was measured after recrystallization at 250 °C.

In this study, we *focus* our modeling efforts on higher stress conditions where GBS is expected to be absent as the most appropriate cases to study the effect of dislocation climb on the texture evolution and strain anisotropy. Strictly speaking, the VPSC-CLIMB modeling strategy we employ strictly enforces equilibrium and compatibility between each individual grain and the surrounding homogeneous effective medium, and therefore, cannot be used to investigate GBS directly. Like <c+a> slip, the activation of GBS has been held responsible for the aforementioned reduction in r-value in AZ31B and alteration of texture[14,37]. Therefore, it is of interest to investigate the impact of including the kinematics of dislocation climb on the results of crystal plasticity modeling of deformation under similar conditions.

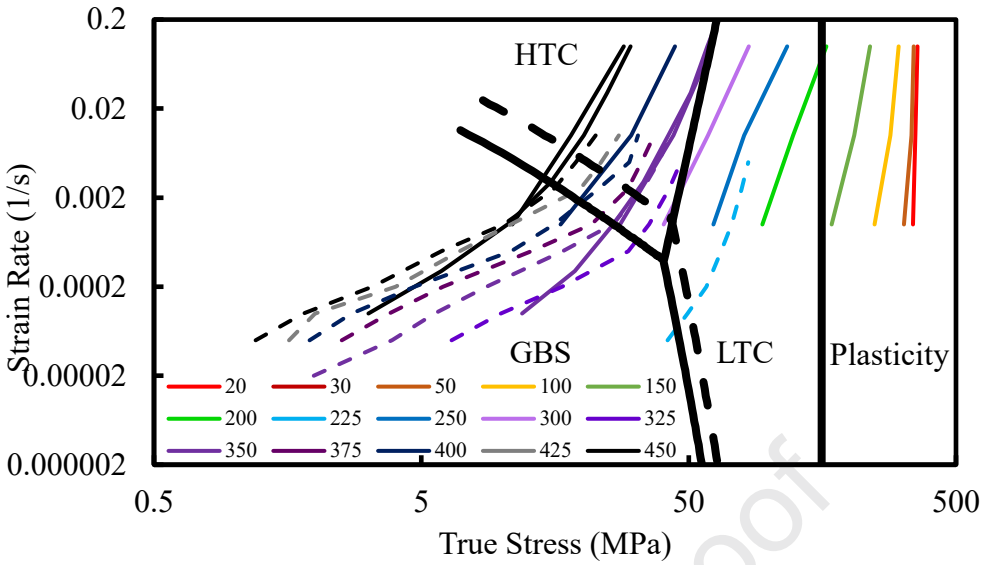

Figure 1: Comparison of constituti ve data from Antoniswamy et al.[14](solid lines), Abu-Farha & Khraisheh [45](dashed lines). The thick black lines denote the boundaries of each deformation mechanism (high temperature creep (HTC), low temperature creep (LTC), grain boundary sliding (GBS), and plasticity) for different grain sizes - Antoniswamy et al.[14](solid) and Abu-Farha & Khraisheh [45](dashed).

4- Experimental and Modeling Methods

Material

Sheets of rolled magnesium alloy AZ31B (designated "X" in [15]) were received from Magnesium Elektron North America in the O temper with a nominal thickness of 1 mm. The composition of the AZ31B sheet was characterized by energy dispersive spectroscopy (EDS) to be 2.9 wt% Al, 0.95 wt% Zn, 0.53 wt% Mn, balance Mg. The Mn content is slightly higher than typically observed (but still within reasonable bounds). Linear intercept measurements done with optical microscopy yielded an average grain size of 8.3 µm and x-ray diffraction performed on the samples identified an α-Mg phase with small amounts of Mn-rich precipitates.

Mechanical Testing

ASTM E-8 subsized samples of rolled Mg alloy AZ31B sheet obtained in the O-temper condition had a gage length of approximately 25 mm, a width of 6 mm and thickness of 1 mm with gage parallel (RD) or perpendicular (TD) to the rolling direction. 5 roughly equally sized regions were marked along the gage length to ensure accurate post-deformation strain measurements. Uniaxial tensile tests were performed on the samples using an MTS Sintech 10\GL load frame and an ATS 3610 split furnace operating at various temperatures (20 - 350°C) and strain rates (10^{-5} - 10^{-1} s^{-1}). Error bars were generated by taking into account the load cell sensitivity (± 5 MPa) into the measured values of stress. Testing conditions were selected to rather evenly span a range of the temperature compensated strain rate known as the Zener-Hollomon parameter

$$Z = \dot{\varepsilon} \exp\left(\frac{Q}{RT}\right) \qquad \text{Equation 1}$$

where $\dot{\varepsilon}$ is the strain rate, Q is the activation energy, R is the universal gas constant, and T is the temperature on an absolute scale. After deformation to ~ 10%, the final dimensions for each of the aforementioned 5 regions were measured and the true plastic strain was determined, along with an average strain level and standard deviation of the strains within the gage. The r-values were used to quantify the anisotropy during deformation,

$$r = \frac{\varepsilon_w}{\varepsilon_t} \qquad \text{Equation 2}$$

where ε_w is the true plastic strain in the width direction and ε_t is the true plastic strain in the thickness direction. Some tensile tests were run to ~30% strain, in order to gain more information about the texture and r-value evolution at the higher temperatures.

Texture Collection and Analysis

Tensile samples were prepared for texture analysis through a series of polishing steps with SiC polishing pads, culminating with a chemical polish of 2% Nital (2% by volume nitric acid in methanol) and a methanol rinse. Texture measurements were collected from samples deformed to ~10% strain at selected Z conditions (and subsequently polished to mid-thickness) using a Panalytical X'Pert Pro diffractometer with a Cu K_α X-ray tube operating at 45 kV and 40 mA in point focus mode on a 5° × 5° measurement grid of tilt and azimuth angles. Texture measurements were also collected on select samples deformed to ~30% true plastic strain in order to study texture evolution to higher strain levels. Regardless of sample orientation, RD was always aligned with the goniometer to ensure that sample coordinates line up with pole figure and simulation coordinates. MTEX, a Matlab toolbox, was used to plot experimental (0002), $(10\bar{1}0)$ and $(10\bar{1}1)$ pole figures and compute Orientation Distribution Functions (ODFs) [47]. Defocusing, background corrections, and pole figure normalization were also performed using MTEX. The resulting ODFs were discretized to obtain 2,000 equally weighted orientations ("grains") with a kernel size of 10° arranged in orientation space to best represent the initial texture, which were in turn used as input for the VPSC-CLIMB simulations described below.

Figure 2 shows the initial texture of the rolled AZ31B sheet measured in this study as the $\varphi_2 = 0°$ slice of the ODF (Bunge Euler angle convention (φ_1, Φ, φ_2)). There are many appropriate representations of texture, including: 3 complete, recalculated pole figures, a single 2-D ($\varphi_2 = 0°$) section of the ODF (Bunge Euler angle convention (φ_1, Φ, φ_2)), and the complete ODF presented in the fundamental zone of Rodrigues (axis/angle) space with hexagonal crystal and orthotropic sample symmetry enforced. Pole figures are the most common texture representation used in the Mg alloy literature due the way in which bulk textures are frequently measured using x-ray or neutron diffraction. Note that the current pole figures of the initial texture (not shown in the interest of space) are identical to those reported previously for the same sheet material [15].

A major drawback of pole figures is that the intensity at a location within a pole figure is not due to a single orientation; it is the integration of the intensity within the ODF along a path of *many* different orientations within orientation space, which all share a particular spatial and crystallographic rotation axis [48]. This is rectified by generating an ODF from experimentally collected pole figures to describe the orientations of each grain. Figure 2 shows several sections

of the ODF at constant φ_2 (per Bunge's convention). This presentation highlights the fact that even the initial texture has some preferred alignment of the $\langle 10\bar{1}0 \rangle$ directions of the crystals with the RD. This is not immediately obvious from the pole figures. The $\varphi_2 = 0°$ slice was deemed representative of the texture in rolled AZ31B since no additional texture components are revealed in the other slices. The apparent shift in the peak intensity positions is a result symmetry and the curved boundaries of the fundamental zone in the employed Euler space. (The nodes are in symmetrically equivalent positions [49].) In fact, even the two nodes present in the $\varphi_2 = 0°$ slice are symmetrically equivalent.

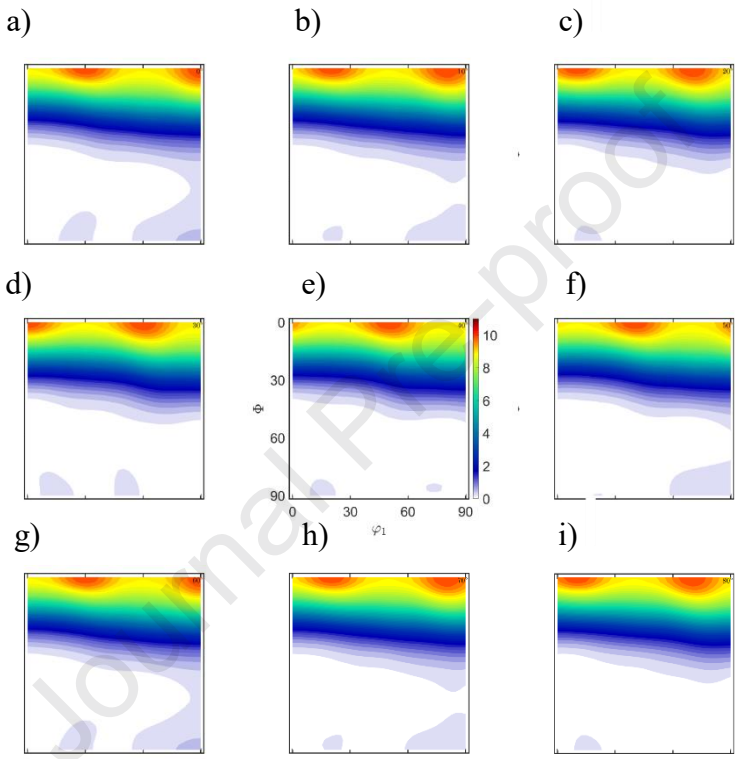

Figure 2: The ODF of as-rolled AZ31B is presented as slices of Euler space (Bunge convention) in 10° increments of φ_2 (a) = 0°, b) = 10°, c) = 20°, d) = 30°, e) = 40°, f) = 50°, g) = 60°, h) = 70°, i) = 80°). Note that the texture intensity is relatively constant along φ_2 and the same texture component is present in all slices, only the location of the node changes. (One of the nodes shown in the ODF slices is symmetrically equivalent to the other due to the curved nature of the fundamental zone in Euler space [49]). Thus, all textures will be presented as ODF slices when $\phi_2 = 0°$. The same intensity scale and axes are used on all texture plots presented in this paper.

Crystal Plasticity Modeling

Figure 3 defines a dislocation-level, local coordinate system used in the following schematic illustrations of the distortions produced by a) glide, b) climb of an edge dislocation, c) cross-glide of an initially screw dislocation, and d) climb of a mixed dislocation. In general, a crystal will experience a simple-shear distortion as a result of dislocation glide, which involves rigid body rotation (Figure 4a). The Taylor axis about which this rotation takes place is given by the cross product ($\widehat{\boldsymbol{b}} \times \widehat{\boldsymbol{n}}$) of the Burgers vector direction $\widehat{\boldsymbol{b}}$ and the slip plane normal vector $\widehat{\boldsymbol{n}}$. The situation is different for the non-conservative, diffusion-controlled climb of edge dislocations of the same slip mode. Such climb induces pure shear, i.e. stretch with no accompanying rigid body rotation (Figure 4b). The climb of mixed dislocations, however, will induce a rigid body rotation consistent with the cross slip of a dislocation (Figure 4c) whose Burgers vector is equivalent to its screw component (Figure 4d). Depending upon the boundary conditions of the crystal, the aforementioned rigid body rotations (plastic spin) will often cause the lattice to rotate around a distinct Taylor axis ($\widehat{\boldsymbol{b}}_{\boldsymbol{s}} \times \widehat{\boldsymbol{\chi}}$), where $\widehat{\boldsymbol{b}}_{\boldsymbol{s}}$ corresponds to the screw portion of the dislocation and $\widehat{\boldsymbol{\chi}}$ corresponds to the normal to the plane of dislocation climb/cross-glide, i.e., the extra half-plane. For example, when mixed dislocations with <a> type Burgers vectors climb, they will induce lattice rotations similar to that of prismatic glide, except these rotations will be proportionally less, for a given amount of dislocation motion, due to the fact that the rotations correspond solely to the screw component of the climbing dislocations. This is in contrast to the case of glide, where both edge and screw portions give rise to the same rotations. In summary, and as originally shown in Lebensohn et al. [19], the rate of texture evolution caused by climb motion is slower than that of the same amount of glide motion.

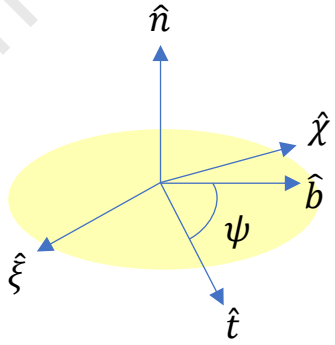

Figure 3: Coordinate system for considering the forces on dislocations within VPSC-CLIMB. $\hat{n}$ is the glide plane normal, $\hat{b}$ is the burgers vector, $\hat{t}$ is the line direction, $\hat{\chi}$ is the climb plane normal and $\hat{\xi} = \hat{b}\, x\, \hat{n}$. ψ is the angle that defines the character of the dislocation.

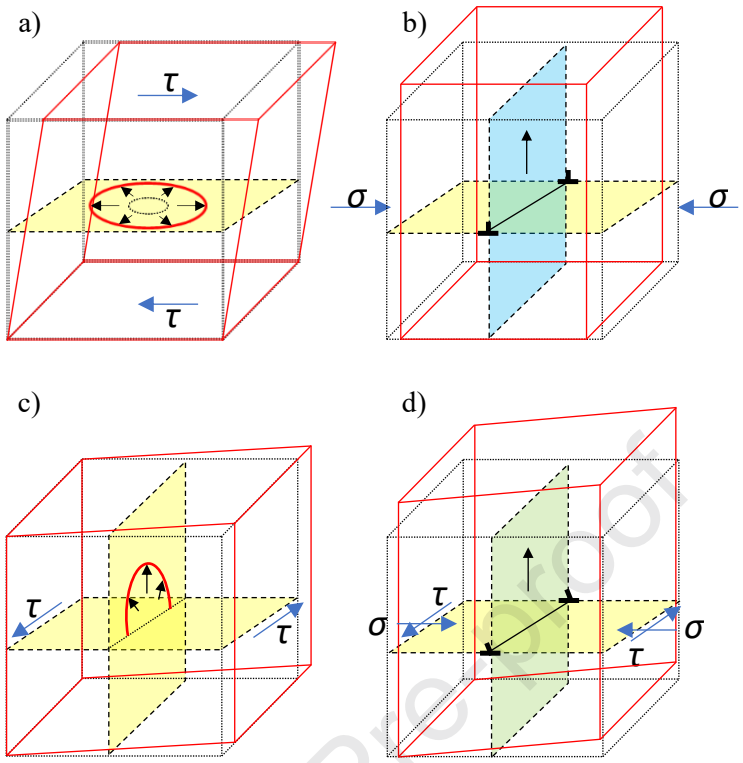

Figure 4: Schematic illustration of the distortions imparted by: a) glide of a basal dislocation, b) climb of a basal edge dislocation, c) prismatic cross-slip of a basal dislocation, and d) climb of a mixed basal dislocation. In each case, the Burgers vector of a basal dislocation is of <a> type. The black arrows within the plane of motion indicates the direction of dislocation motion. Glide (yellow) and climb (blue) planes are shown in each figure for orientations purposes. The climb plane for mixed dislocations is denoted as green to show that the motion is a combination of prism glide and basal climb.

The crystal-level constitutive model parses the viscoplastic (*vp*) strain rate into two parts, that due to glide (*g*) and that due to climb (*c*).

$$\dot{\varepsilon}_{ij}^{vp} = \dot{\varepsilon}_{ij}^{g} + \dot{\varepsilon}_{ij}^{c} \qquad \text{Equation 3}$$

As discussed previously, a complete deformation may involve a combination of stretch and rigid-body rotation. Equation 4 provides the well-known relationship between the deformation rate tensor, $\dot{\boldsymbol{\varepsilon}}^{g}$ (boldface denotes a tensor), the shear rate on the s^{th} slip system, $\dot{\gamma}^{g,s}$, and the Schmid tensor, $\boldsymbol{m}^{s}$, which is the symmetric portion of the dyadic cross product of the slip direction and slip plane normal unit vectors, $sym\left(\hat{\boldsymbol{b}}^{s} \otimes \hat{\boldsymbol{n}}^{s}\right)$.

$$\dot{\varepsilon}_{ij}^{g} = \sum_{s} \dot{\gamma}^{g,s}\, m_{ij}^{s} \qquad \text{Equation 4}$$

Similarly, Equation 5 gives the associated plastic spin (or rate of rotation) in terms of the slip system shear rates and the antisymmetric portion of the same dyadic product, denoted q_{ij}^{s}.

$$\dot{\omega}_{ij}^{g} = \sum_{s} \dot{\gamma}^{g,s}\, q_{ij}^{s} \qquad \text{Equation 5}$$

The shear deformation rate due to dislocation climb can be expressed similarly to Equation 4

$$\dot{\varepsilon}_{ij}^{c} = \sum_{s} \dot{\gamma}^{c,s}\, k_{ij}^{d,s} \qquad \text{Equation 6}$$

where $\boldsymbol{k}^{d,s}$ is the deviatoric portion of the symmetric part of the Hartley climb tensor, $\boldsymbol{k}^{s} = sym\left(\widehat{\boldsymbol{b}}^{s} \otimes \widehat{\boldsymbol{\chi}}^{s}\right)$, and $\widehat{\boldsymbol{\chi}}^{s}$ denotes the positive glide direction (or climb plane normal direction) [50]. There is a distinction between climb, which in principle can give rise to both deviatoric strain and dilatation, and glide which can only produces deviatoric strain. We will return to the issue of dilatational strains in the discussion section. For now, it suffices to say that the dilatation concerns local fluctuations in vacancy concentration. These fluctuations do not have an appreciable impact upon the net strain of the crystal, and, hence, are not addressed in Equation 6. Similar to Equation 5, Equation 7 gives the plastic spin that occurs due to dislocation climb.

$$\dot{\omega}_{ij}^{c} = \sum_{s} \dot{\gamma}^{c,s} r_{ij}^{s} = \frac{1}{2}\sum_{s} \dot{\gamma}^{s} \cos(\psi^{s}) \left(b_{j}^{s}\xi_{i}^{s} - b_{i}^{s}\xi_{j}^{s}\right) \qquad \text{Equation 7}$$

where ψ^{s} is the angle between the Burgers vector and the line direction (Figure 3), which defines the character of the average dislocation climbing from the slip system, *s*, and $\boldsymbol{r}^{s}$ is the skew symmetric portion of the Hartley climb tensor [50]. In principle, ψ^{s} could evolve with deformation, but we presently assign it to be a constant value in all of the simulations of the present study. Specifically, we examine three cases. The first, $\psi^{s} = \frac{\pi}{2}$, indicates that all of the climbing dislocations are of pure edge character. This is a limiting case, since all such climb will accommodate strain without causing any lattice rotation. Considering another limiting case, $\psi^{s} = 0$, involving dislocations of solely screw character, it is shown that Equations 6 and 7 can be used to describe the kinematics of prismatic cross-glide of <a> dislocations as well as climb. This is an interesting case for Mg alloys in which screw dislocations with an <a> Burgers vector are the same ones which are responsible for prismatic slip. The results obtained for this case were indistinguishable from those in which prism slip with the same critical stress is employed.

Up to this point, only the kinematics has been discussed for simplicity. The strain rate caused by dislocation glide is understood to have an exponential dependence upon stress [51],which can be approximated as a power law, over a limited range of strain rates.

$$\dot{\varepsilon}_{ij}^{g} = \dot{\gamma}_{0} \sum_{s=1}^{N_s} m_{ij}^{s} \left(\frac{|\boldsymbol{m}^{s}:\boldsymbol{\sigma}'|}{\tau^{g,s}}\right)^{1/m_g} sgn(\boldsymbol{m}^{s}:\boldsymbol{\sigma}') \qquad \text{Equation 8}$$

where $\dot{\gamma}_{0}$ is the reference shear strain rate (which was set equal to the applied strain rate of the test), m_g the rate sensitivity governing glide is assumed equal to 1/20 in the present study (high

enough to distinguish it from climb, yet low enough to ensure ready convergence[1]), and $\tau^{g,s}$ is the critical resolved shear stress of the s^{th} slip system. Dislocation glide only depends on the deviatoric portion of the stresses applied to the crystal, $\boldsymbol{\sigma'}$. At the dislocation level, one can consider the generalized Schmid law $\boldsymbol{m^s}:\boldsymbol{\sigma'}$ as related to that portion of the Peach-Kohler force which lies within the glide plane, i.e., $f_g = \boldsymbol{f}\cdot\hat{\boldsymbol{\chi}}^s = (\boldsymbol{m^s}:\boldsymbol{\sigma'})b$.

The constitutive relationship used to describe climb is similar to the one employed for glide [19]

$$\dot{\varepsilon}_{ij}^{c} = \dot{\gamma}_0 \sum_{s=1}^{N_s} k_{ij}^{d,s} \left(\frac{\left|\boldsymbol{k^{d,s}}:\boldsymbol{\sigma'}\right|}{\sigma^{c,s}} \right)^{1/m_c} sgn\left(\boldsymbol{k^{d,s}}:\boldsymbol{\sigma'}\right) \qquad \text{Equation 9}$$

where $k_{ij}^{d,s}$ functions analogously to m_{ij}^{s}, $\sigma^{c,s}$ is a critical stress for climb analogous to $\tau^{g,s}$ for glide, and m_c is the rate sensitivity governing climb. Again, this expression can be rationalized in terms of the component of the Peach-Kohler force on a dislocation which is normal to the glide plane, i.e., $f_c = \boldsymbol{f}\cdot\hat{\boldsymbol{n}}^{\boldsymbol{s}} = (\boldsymbol{k^s}:\boldsymbol{\sigma'})b$. As written, Equation 9 ignores the effect of hydrostatic pressure on dislocation climb. The possible effect of pressure is taken up in the discussion and will be revealed negligible for the current study. In theory, n_c and $\sigma^{c,s}$ are temperature dependent, but $m_c = 1/3$ is taken as a constant in the power law regime. Again, the implications of these choices will be addressed in the discussion section. The optimal CRSSs (including $\sigma^{c,s}$) relative to basal glide are determined from minimizing a total residual error objective function, as described below.

The glide critical resolved shear stress evolves per the empirical Voce strain hardening relationship [52].

$$\tau^{g,s} = \tau_0^s + \tau_1^s \left(1 - \exp\left(-\Gamma \left|\frac{\theta_0^s}{\tau_1^s}\right|\right)\right) \qquad \text{Equation 10}$$

where $\Gamma = \sum_s \Delta\gamma^s$ is the accumulated shear in the grain; τ_0^s is the initial CRSS, θ_0^s is the initial hardening rate, and $(\tau_0^s + \tau_1^s)$ is the back-extrapolated CRSS. As a first-order approximation, the critical stress for climb ($\sigma^{c,s}$) is assumed to remain constant at a given temperature and strain rate. It is acknowledged that more rigorous treatments of the hardening evolution have been developed, based upon evolution of the dislocation density [53]. However, this simpler approach has been adopted in the present inaugural attempt to incorporate the effects of dislocation climb kinematics into the polycrystal plasticity modeling of Mg alloy deformation.

The VPSC model [12], adapted to account for the kinematics of dislocation climb (VPSC-CLIMB) as summarized above, was used to simulate the experimentally measured textures and r-values. For a complete discussion of the model, readers are directed to the original articles [19,54]. VPSC employs an explicit strain integration scheme, and hence, straining increments were maintained as 0.002 in order to avoid error accumulation. By comparing the simulated results with experimentally measured values, mechanistic understanding regarding the transition

[1] Recent advancements in the numerical techniques employed in crystal plasticity modeling allow for more realistic (even lower) values [76,77] were not employed in this first exploration of climb effects.

from low to high temperature deformation behavior of an archetypal Mg alloy AZ31B is obtained.

Parametric study

The root mean squared difference between the experimental and simulated textures is chosen as a means of quantifying the level of agreement per

$$TexErr = \sqrt{\int \left(f_{exp}(g) - f_{sim}(g)\right)^2 dg} \qquad \text{Equation 11}$$

where $f_{exp}(g)$ refers to the orientations that comprise the experimental ODF and $f_{sim}(g)$ refers to the orientations belonging to the simulated ODF. This is akin to calculating the norm of the difference between the experimental and simulated ODFs or the standard deviation of a dataset using statistics. This is, in fact, a *relative* error because the ODFs are normalized to unity, $\int f(g)dg = 1$. The typical average texture "error/change" between deformed samples and the initial rolled texture was found to be 0.3, providing a sense of the magnitude of this texture measure. A metric for the total residual error between the experiment and simulation, including texture and strain anisotropy (r-values) provides an objective function

$$f_0 = w_{Tex}(TexErr_{TD} + TexErr_{RD}) + w_r\left(\frac{\left|r_{sim} - r_{exp}\right|_{TD}}{r_{TD\_exp}} + \frac{\left|r_{sim} - r_{exp}\right|_{RD}}{r_{RD\_exp}}\right) \qquad \text{Equation 12}$$

for both RD and TD sample orientations. The errors in texture are weighted more strongly than the r-values ($w_{Tex} = 0.75\ vs.\ w_r = 0.25$) because the texture showed more specificity than the r-values. Each slip mode has a unique texture evolution (through the distortion created by dislocation motion) for the initial rolled texture (Figure 4), but some have similar effects on r-value.

Final best-fits of the VPSC-CLIMB model to the cases of greatest interest were obtained by varying the model pararameters (the critical resolved shear and normal stresses of the various modes under consideration) using a genetic algorithm (GA) [55,56] to minimize the objective function (Equation 12). This novel approach adjusts CRSS values to match simulations to the experimental evidence of dislocation kinematics (texture evolution and strain anisotropy) rather than past attempts which have attempted to match macroscopic stress-strain tests [57]. On average, ~ 800 (32 simulations per generation × 10-15 generations × 2 repetitions of the genetic algorithm (one coarse and one fine search) simulations were run per experimental test condition; therefore simulations were run in parallel to increase computational efficiency.

5- Results

Constitutive behavior

Figure 5a shows the effect of temperature and sample orientation (RD vs. TD) on the stress-strain behavior of AZ31B tested in the current study. The flow stresses and strain hardening rates were observed to decrease with increasing temperature, as observed with prior studies [3,14,15]. The flow stress at a strain of 0.1, along with the testing conditions, permit the results to be overlaid with the previously introduced Ashby-type deformation mechanism map (Figure 5b). From this presentation, we can highlight the 5 cases that will be examined most closely with an orange ring.

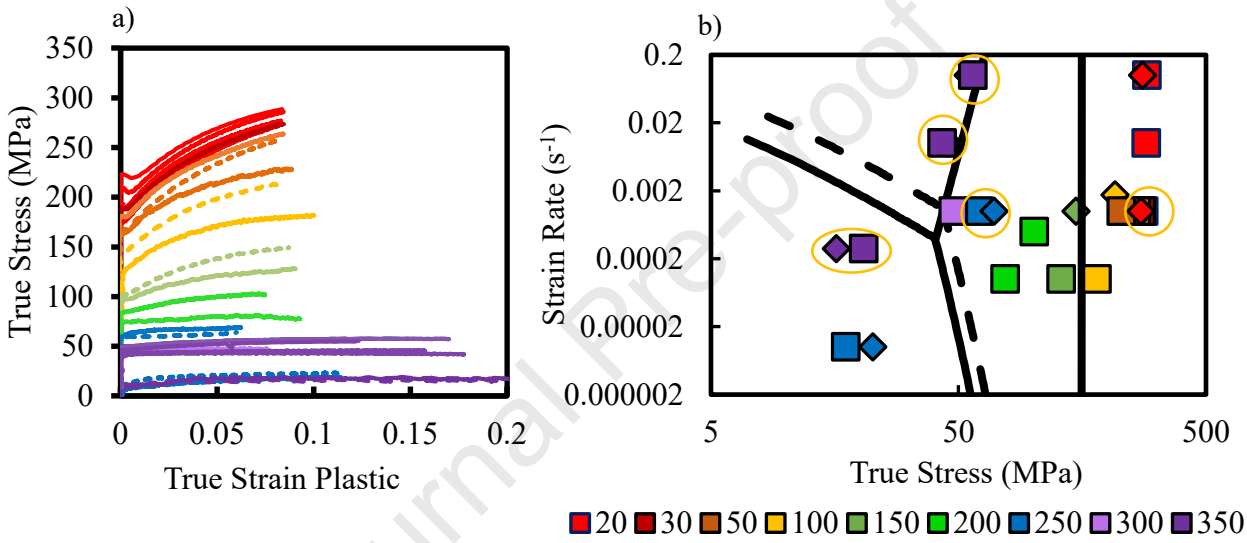

Figure 5: a) Tensile test results (TD = solid lines, RD = dashes), b) Ashby map with current data overlaid.

Although the primary aim of the study is assessing the role of dislocation climb, which may be illuminated through careful examination of kinematics of plasticity (texture evolution and plastic anisotropy), it is also noteworthy to show that if one is more concerned with constitutive flow alone, the empirical [58] model well describes the constitutive response over the entire range explored,

$$Z = \dot{\varepsilon} \exp\left(\frac{Q}{RT}\right) = A[\sinh(a\sigma)]^{1/m} \qquad \text{Equation 13}$$

where A, a, and m are temperature-independent material constants, σ is the flow stress at a strain of 0.1, and Z is the Zener-Holloman parameter introduced in Equation 1. This empirical relationship was proposed to bridge between the low temperature, high strain rate regime which is well described by an exponential and the high temperature, low stress regime characterized by a power law. The "hinge-point" between the two regimes is the condition where $a\sigma = 1$. Although it was originally used to describe the hot deformation behaviors of FCC metals such as

Al, Ni and Cu, it has frequently been shown to yield a good fit with data collected from tensile tests using HCP metals over a wide range of temperatures and strain rates [15,59].

A best fit of the Sellars–Tegart model through nonlinear least squares regression yielded the following parameters: m = 0.23, A = 4.06 x 10^9, α = 7.16 x 10^{-3} and Q = 111 kJ/mol. It should first be noted that the observed constitutive response is generally in agreement with those found previously [14,15,45], albeit over a narrower temperature and strain rate range (Figure 6a). Differences in the near ambient flow stresses are attributed to differences in grain size and temper condition. Differences in the strain rate sensitivity of prior studies by one of the present authors are attributed to previously using an assumed activation energy of 140 kJ/mol [15], rather than fitting it as was done here. For conditions where ln(Z) > 23, the dependence of the strain rate on stress is well approximated as exponential, and in the range ln(Z) < 23, the data may be described by a power law expression with a slope of 4.36 (indicative of climb-and-glide creep behavior). If one takes the log of both sides of the above empirical expression (Equation 13) and takes the derivative with respect to ln(σ) at a fixed temperature, one can determine the instantaneous strain rate sensitivity, m. At high temperatures (i.e., within the power law regime (> 200 °C (~0.5T_M))), m = 0.23, and at ambient conditions of 293K and a nominal strain rate of 1x10^{-3} s^{-1}, the strain rate sensitivity decreases to m ~ 1/70 = 0.014.

In addition to the observed decrease in the flow stress and increase in strain rate sensitivity, the strain anisotropy (as indicated by the r-value given in Equation 2) undergoes a characteristic decrease with decreasing Z (Figure 6b). Both RD and TD tensile conditions exhibit a low temperature plateau followed by a gradual decline until the samples exhibit isotropic strain behavior (i.e., r = 1) with the only difference being that the low temperature plateau is at a higher level for TD than it is for the RD case. This is due to details of the typical rolling texture in AZ31B-O temper sheet/plate material in which the main basal texture component is tipped slightly more toward the RD than it is the TD. This promotes a higher activity of prismatic slip in the TD case [3]. Interestingly, there is a gradual decline in strain anisotropy with decreasing Z, reaching isotropy in the power law creep regime (ln(Z) < 23). Historically, power law creep has been understood to be controlled by dislocation climb and glide [13]. This observation, along observations related to texture evolution discussed below, caused the present authors to begin questioning the earlier conclusion that increased activation of <c+a> slip is the reason why the r-values of Mg alloys tend to decrease at higher temperatures [3].

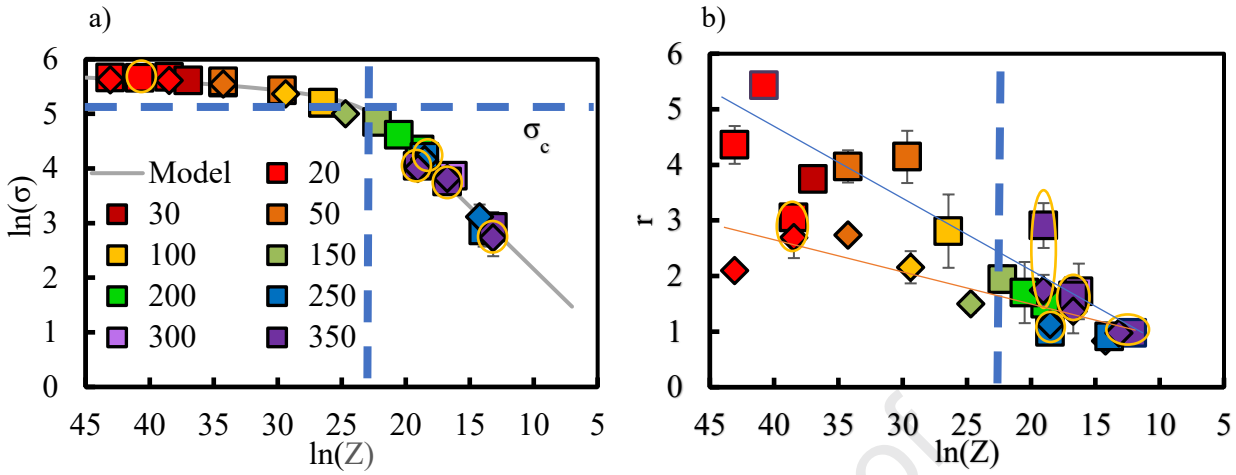

Figure 6: a) flow stress (at ε ~ 0.1) and b) r-value as a function of testing conditions (strain rate, temperature and sample orientation (RD = diamond, TD = square). The dashed line in 6a shows the critical stress between the exponential and power law regimes. Vertical dashed lines denote the approximate transition into power law creep as defined by the critical stress. The blue and orange lines in b) serve as guides to the eye for the reduction in r-value for TD and RD sample, respectively.

Texture Evolution and Anisotropy at Ambient Temperatures – Experiment and Simulation

The main texture component of the low temperature TD tension texture after 10% strain (Figure 7a) is rotated about the z-axis of Euler space (from $\phi_1 = 30°$ to 0°) and strengthened relative to the initial rolled and annealed texture presented in Figure 2, whereas the main texture component of the as-received material is simply strengthened after uniaxial tension deformation along the RD (Figure 7c). This rotation about the sample z-axes (in both cases) is because the initial "basal" texture has a preferred orientation which places the crystals' c-axes nearly parallel to the sheet normal direction. The slip mode which is responsible for this characteristic rotation about the crystals' c-axes is prismatic slip. The relatively high r-values observed at low temperature are another characteristic of prismatic slip in these basal-textured sheets.

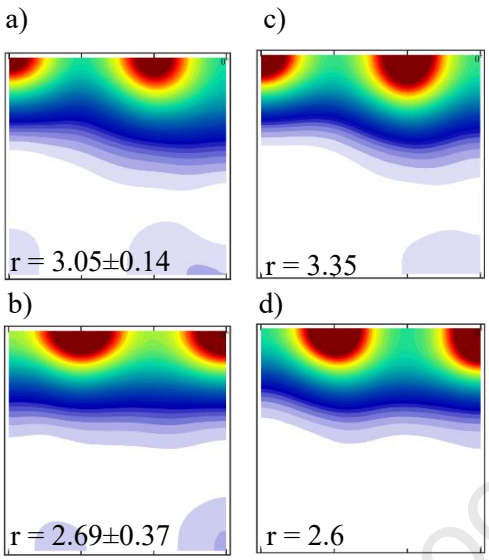

Figure 7: The importance of the prismatic slip of <a> dislocations during room temperature tensile testing (20 °C, 0.001 s^{-1}) is indicated by the appearance of a node-like component in the texture and higher r-values of both the experiments and simulations of tension along (a) & (b) TD and (c) & (d) RD directions, respectively.

As described earlier, minimization of the objective function (Equation 12) was performed using a genetic algorithm to obtain a best-fit simulations of the observed r-values (Figure 6b) and textures of TD and RD samples (Figures 7a & 7c, respectively). Once the ratios of the relative strengths were obtained by the aforementioned optimization process, the Voce strain hardening parameters (Equation 9) required to model the low temperature response (i.e., at temperatures where climb activity is insignificant) were fit and are reported in Table 1. Notably, values for prism and <c+a> slip determined for RT deformation are similar to those used in previous studies [9]. In all conditions of interest, the global minimum in the objective function corresponded to a high CRSS value for twinning, which corresponds to the fact that most of the grains are unfavorably oriented for twinning during in-plane tension, making that parameter rather unconstrained. These optimized parameters for low temperature simulations yield *a* *TexErr* = 0.29 for RD and *TexErr* = 0.26 for TD orientations (resulting in an overall error of f_0= 0.45). The simulations confirm that the dominant slip mechanism during low temperature tensile deformation of basal textured sheets is prismatic slip, with smaller contributions from basal and <c+a> slip and tensile twinning.

Table 1: Voce hardening parameters for low and high temperature simulations

	LT (20°C, 10^{-3} s^{-1})			LTC (250°C, 10^{-3} s^{-1})			LTC/HTC Boundary (350°C, 10^{-1} s^{-1})		HTC (350°C, 10^{-2} s^{-1})		GBS (350°C, 2.8 x 10^{-4} s^{-1})	
	τ_0	τ_1	θ_0	τ_0	τ_1	θ_0	τ_0	τ_1	τ_0	τ_1	τ_0	τ_1
Basal Glide	35.4	10.5	300.	15.	2.	300.	16.6	0.49	19.3	0.5	5.92	2.2
Prism Glide	76.7	96.4	300.	24.5	4.5	300.	18.5	4.5	20.	4.4	16.78	6.24
<c+a> Glide	96.4	111.5	300.	24.6	6.3	300.	26.2	3.8	37.2	5.6	23.87	8.77
<a> Climb	n/a	n/a	n/a	29.4	0.0	0.	45.1	0.0	21.3	0	8.96	0
Tensile Twinning	118.3	21.	300.	34.9	2.6	100.	51.2	1.	35.5	0.5	14.49	4.97

Texture Evolution and Anisotropy at Elevated Temperatures – Experiment and Simulation

As the Zener-Holloman parameter is decreased from 40 down to around 10, the dominant mechanism changes from low temperature plasticity to power law creep to GBS (Figures 5 & 6). Figure 8 shows an example of how the corresponding texture strength decreases. Compare the experimental textures in Figures 8a and 8c with those presented in Figures 7a and 7c. These results suggest that the activity of the non-basal, prismatic slip mode responsible for the texture evolution and high r-values which are characteristic at low temperatures is decreased. Measurements repeated at a higher strain level (~30%) reveal only a modest evolution of the texture and r-values between 10 and 30% strain (Figure 8). The features which do evolve are similar to those observed at lower strains at ambient temperature, which is consistent with the continued but lower relative activity of prismatic slip of <a> type dislocations. One thing to note from these results and the original results of Agnew & Duygulu [3] is that the experimental textures obtained after high temperature deformation do not exhibit a signature feature of extensive <c+a> slip, a splitting of the basal texture toward the tensile direction, a point which will discussed further below.

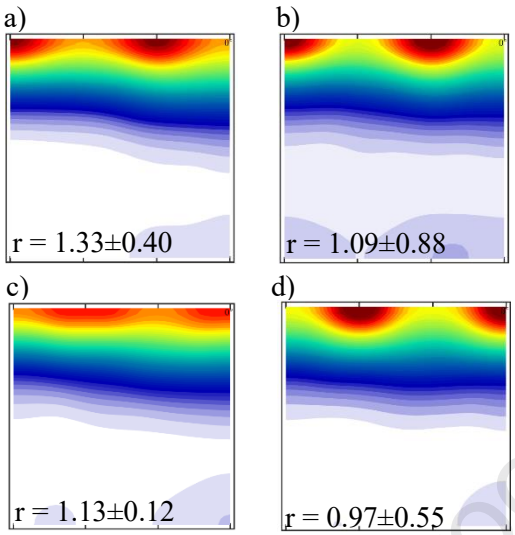

Figure 8: Experimental deformation textures observed after straining at a rate of 0.001 s^{-1} at 250 °C to various strain levels: a) & c) 0.1 and b) & d) 0.3 for each orientation (TD – a) & b) and RD – c) & d)). Note that the textures continue to evolve with strain toward the node like texture shown in Figure 7, due to the continued activation of dislocation glide (i.e., prism slip).

The following results poignantly illustrate the advantage of genetic algorithm (GA) parameter determination and of introducing the kinematics of dislocation climb by comparing the results of three approaches to determine crystal plasticity model parameters to best-fit the case of deformation at 250 °C and a strain rate of 0.001 s^{-1} up to a tensile strain of 0.3:

- parameters taken from the literature [3], which were "hand fit," (Figures 9c & 9d)
- GA without climb (Figures 9e & 9f), and
- GA with climb of <a>-type dislocations (Figures 9g & 9h).

The experimental textures and r-values presented in Figures 8b & 8d and are reproduced in Figures 9a & 9b for ease of comparison with the simulated results. It is clear that the use of a genetic algorithm resulted in a much better fit than the parameters taken from Agnew & Duygulu (f_0 = 1.90 vs 4.64, respectively). The GA method converged to a ratio between the CRSS of <c+a> to prism of 1, the lower bound of the aforementioned CRSS constraint, which resulted in decreased r values and weaker node texture component. However, including climb resulted in another large quantitative improvement (note decrease in error to f_0 = 0.67) as well as qualitative improvement in the general appearance of the textures. The extension of the texture components off the upper edge of the ODF sections of Euler space shown in Figures 9c through 9f are characteristic of the significant activity of <c+a> slip in the simulations, but these features are not observed experimentally. This new, physically-motivated approach provides a definitive improvement over modeling prior strategies and suggests that dislocation climb plays a significant role in strain accommodation over a range of temperature and strain rate regimes (Figures 9 and 10), as detailed further below.

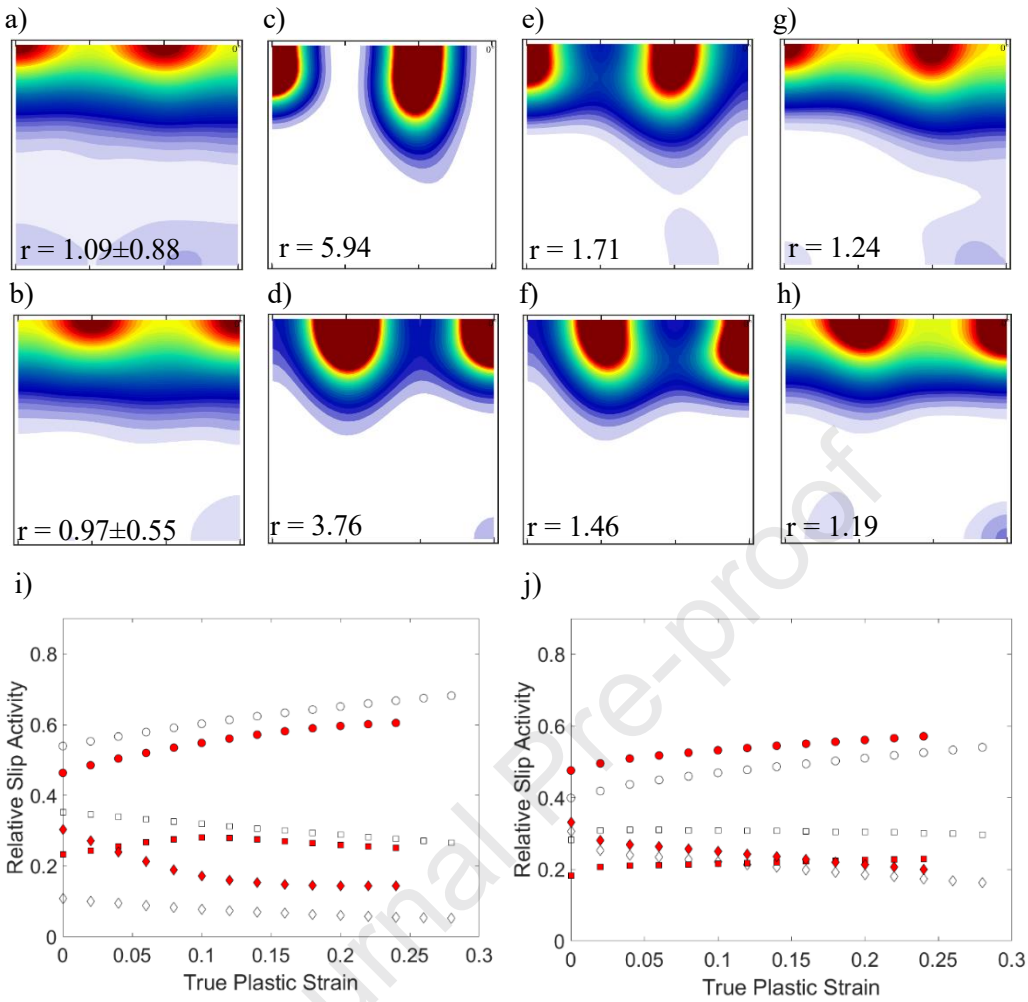

Figure 9: The importance of the climb of <a> dislocations during tensile deformation within the low temperature creep regime (e.g., 250 °C, 0.001 s^{-1}) is indicated by the slower texture evolution and lower r-values of both the experiments and simulations of tension along TD (a,) c), e) and g)) and RD (b), d), f) and h)) directions, respectively. The efficacy of the incorporation of climb and machine learning are demonstrated through comparisons between: a) & b) experimental, c) & d) Agnew & Duygulu (f_0 = 4.64) [3], fits from a genetic algorithm without climb (e) & f)) (f_0 = 1.90) and with climb (g) & h))(f_0 = 0.67). Figures i) and j) show the fraction of strain accommodated by the glide modes activated in Agnew & Duygulu and GA without climb simulations, respectively. The relative slip activity plot for simulations involving climb can be found in Figure 11d). RD = white markers, TD = red markers. Circle = prism slip, square = basal slip and diamond = <c+a> slip.

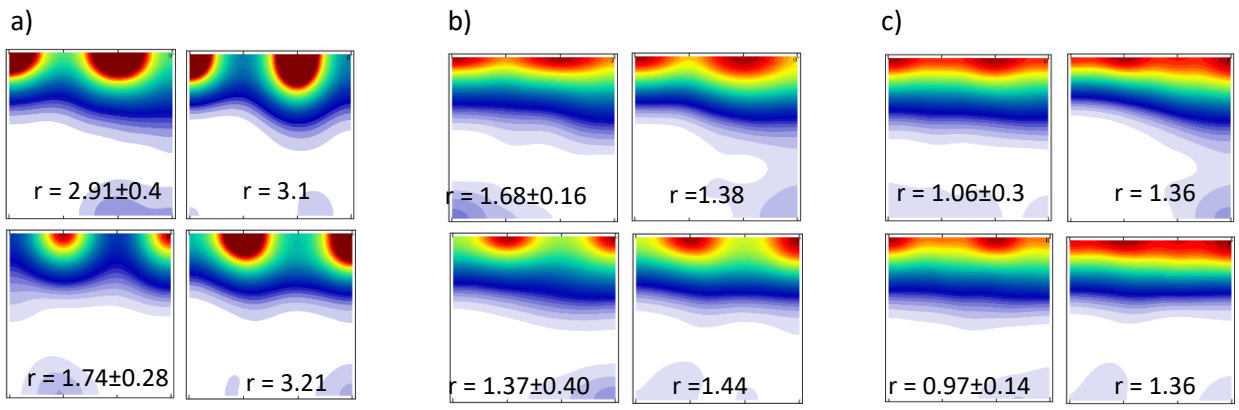

Figure 10: The influence of strain rate on isothermal tensile testing at 350 °C: a) 0.1 s^{-1}, b) 0.01 s^{-1} and c) 0.00028 s^{-1}. Each row (top – TD, bottom-RD) of the block shows the experimental (left) and simulation (right) texture evolutions and associated r-values. Note that the texture evolution diminishes significantly as the strain rate decreases, denoting increased climb activation.

The amount of strain predicted to be accommodated by dislocation climb and glide during elevated temperature tensile tests by the VPSC-CLIMB model shows some expected and surprising trends (Figures 11d and 12d-f). While the samples strained at room temperature (~ $0.3T_m$) do not require strain accommodation by climb, the samples tested at higher temperatures (250°C, 10^{-3} s^{-1} and 350°C, 10^{-1} s^{-1}) do. This is not surprising. On the other hand, those two high temperature cases are predicted to exhibit distinct levels of climb, despite the fact that the two tests were conducted at a similar value of the Zener-Holloman parameter (Equation 1) and have correspondingly similar flow stresses (Figure 6a). This result emphasizes the inadequacy of the traditional constitutive modeling approach, which can capture the variations of flow stress, but does not acount for distinctions in the anisotropy (Figure 6b) and texture evolutions of the two test conditions. For the sample tested at 250°C and 10^{-3} s^{-1}, more than 50% of the strain is predicted to be accommodated by basal <a> dislocation climb, and the rest of the strain is almost equally distributed amongst the glide modes. This is a surprising result, since classical considerations of climb and glide creep typically hold glide responsible for the bulk of the strain accommodation, even in cases where the climb mode is rate controlling (e.g., [60]).

However, the replacement of prism slip, in particular, is essential in order to induce the reduced r-values (r ~ 1.1-1.5) of high temperature deformation. At 350°C, and a strain rate of 10^{-1} s^{-1}, most of the strain is predicted by VPSC-CLIMB to be accommodated by prismatic and basal slip with only a small amount of basal climb activity (Figure 12d), similar to the low temperature results (Figure 11c). This helps to explain why the relatively high r-values and similar texture to that observed at low temperature persist to such a high temperature (Figure 10a). When varying just the strain rate at a fixed temperature of 350 °C, the trend is straightforward. Note the increasing incidence of dislocation climb predicted by VPSC-CLIMB as the strain rate decreases from 10^{-1} to 10^{-2} to 3 x10^{-4} s^{-1} (Figure 12d, 12e, & 12f). At 350°C, ~3 x10^{-4} s^{-1}, which resides within the GBS regime (Figure 5b), the best fit simulation requires ~ 80% of the strain to be accommodated by climb. This is probably not physically accurate; however, it is interesting to note that one can describe many aspects of the response using the present VPSC-CLIMB model.

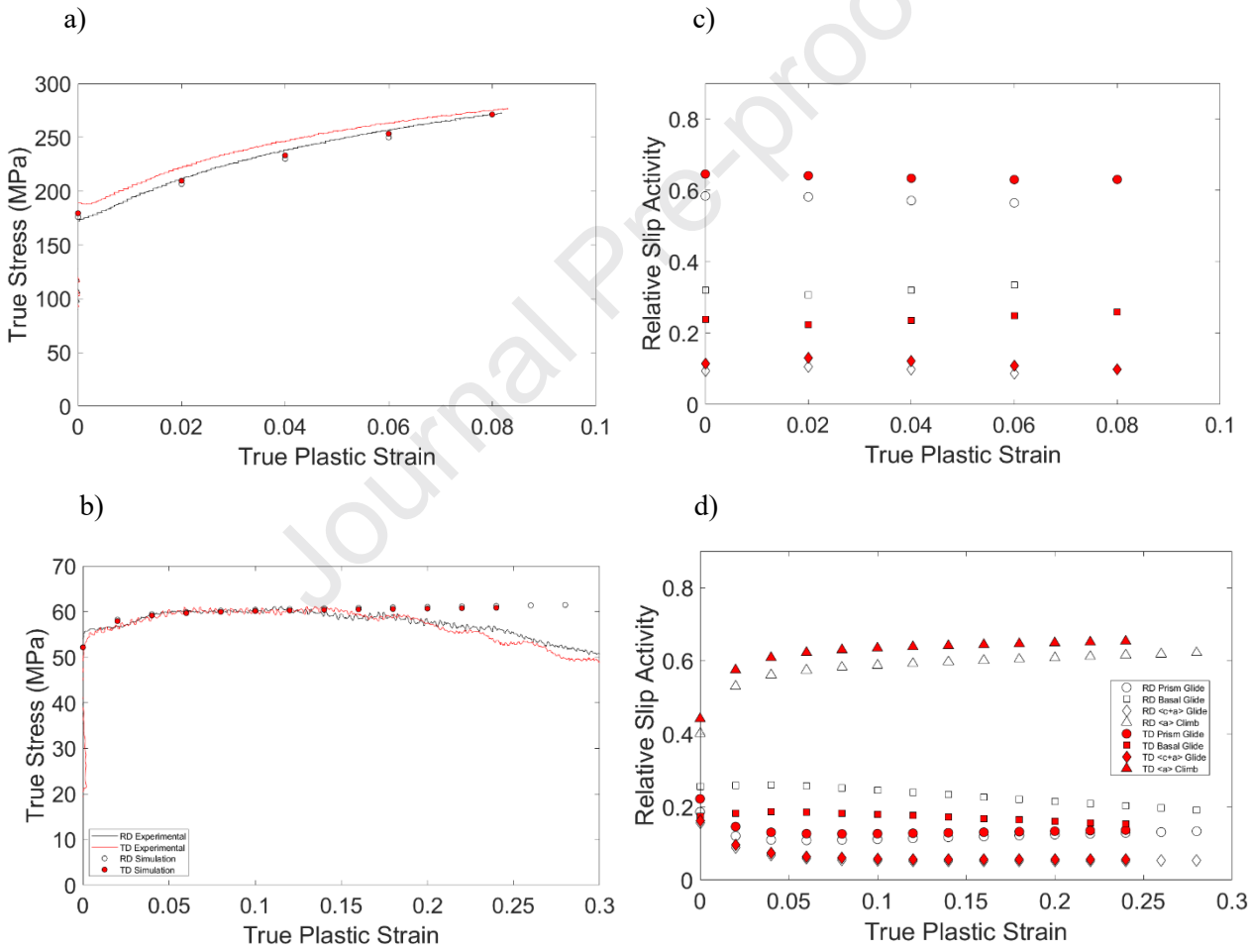

Figure 11: Experimental and simulated stress strain curves: a) Conventional Plasticity (20 °C, 10^{-3} s^{-1}) and b) Low Temperature Creep (250 °C, 10^{-3} s^{-1}) and their respective relative slip (& climb) activity plots: c) Conventional Plasticity (20 °C, 10^{-3} s^{-1}) and d) Low Temperature Creep (250 °C, 10^{-3} s^{-1})

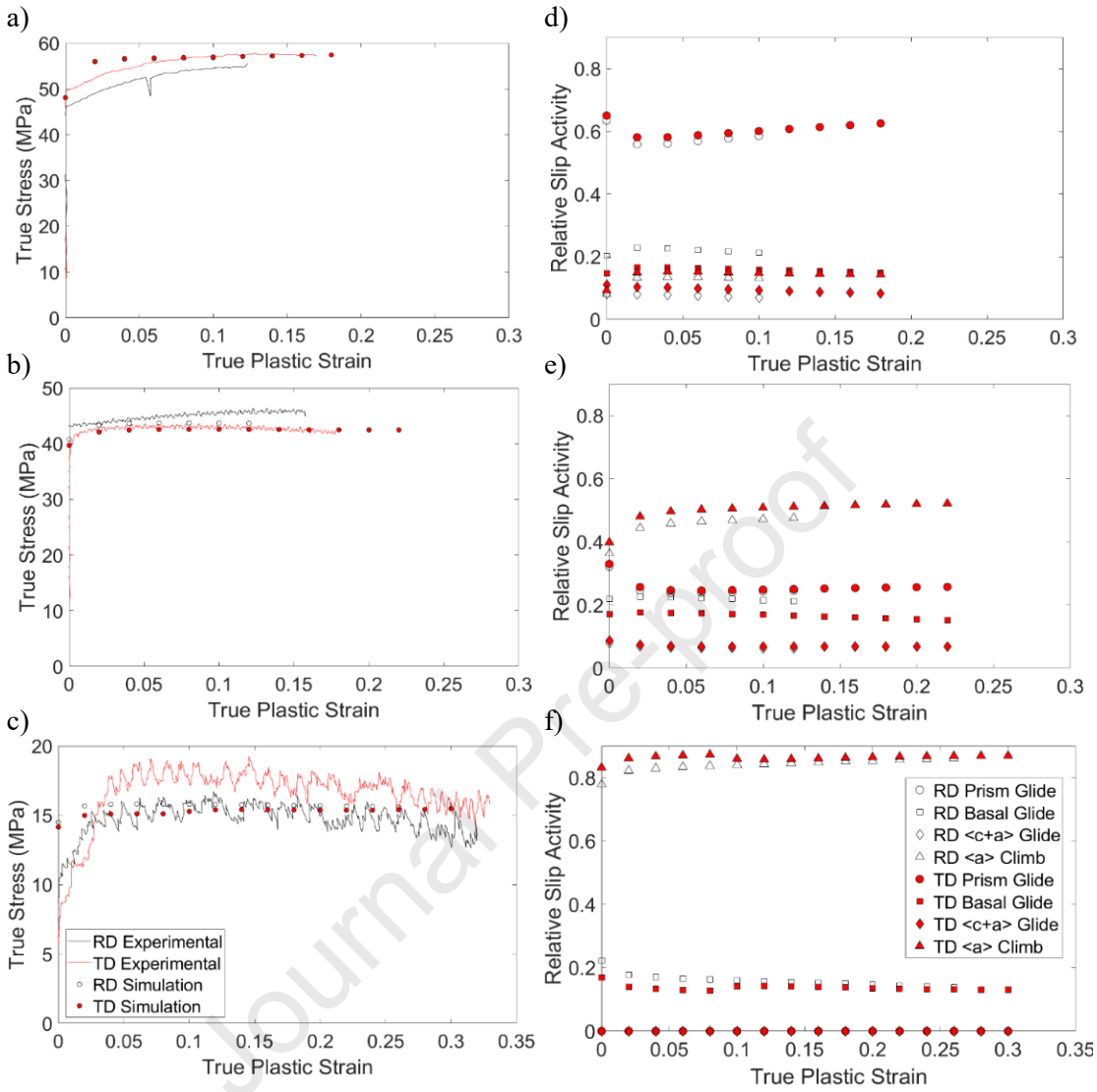

Figure 12: Experimental and simulated stress strain curves (a)-c)) and relative activity plots (d)-f)): Low Temperature Creep/High Temperature Creep Boundary (350 °C, 10^{-1} s^{-1}), High Temperature Creep (350 °C, 10^{-2} s^{-1}) and Grain Boundary Sliding (350 °C, 2.8 x 10^{-4} s^{-1})

Once the best-fit critical stress values (relative to that of basal glide) for the investigated climb and glide modes were obtained by fitting the simulation results to the experimentally measured texture and r-value by minimizing the objective function (Equation 12), the Voce hardening parameters presented in Table 1 were fit to best represent the experimental stress strain curves, as shown in (Figures 11a-b and 12a-c). It is interesting to note that the CRSS values for the non-basal slip and the climb mode obtained by the employed genetic algorithm are only slightly larger than that of basal slip, suggesting that there must be rather balanced activity of all the modes in order to best describe the observed texture and strain anisotropy.

Finally, simulations were performed to examine the effect of the character of the climbing dislocations and their results are summarized here. As suggested previously, "climb" of basal <a> screw dislocations results in identical contributions to the texture and r-value as prism <a> glide (i.e., a texture component that rotates the texture towards $\varphi_1 = 0°$ (TD) or $\varphi_1 = 30°$ (RD) in Euler space and an increase in the r-value). This was shown to be true for both TD and RD simulations in which the "climbing" dislocations were assumed to be 100% <a> type screw dislocations. Relative to the results presented in Figures 9g and 9h, such cross glide simulations (Figure 13) involving the same Voce parameters presented in Table 1 resulted in higher r-values (1.7 vs 1.24 for TD and 1.7 vs 1.19 for RD) and a texture evolution reminiscent of the effect of prismatic glide (node-like texture signatures), when compared to simulations with <a> edge climb. Thus, dislocation character will not be discussed further, since "climb" of screw dislocation behavior can be described by an existing mechanism (i.e., the glide of <a> dislocations on prism planes). This makes the initial assumption of edge-only dislocation climb plausible, though this is a topic which is certainly worthy of further investigation by lower length-scale modeling techniques such as discrete dislocation dynamics (DDD) simulation or experiments such as in-situ transmission electron microscopy.

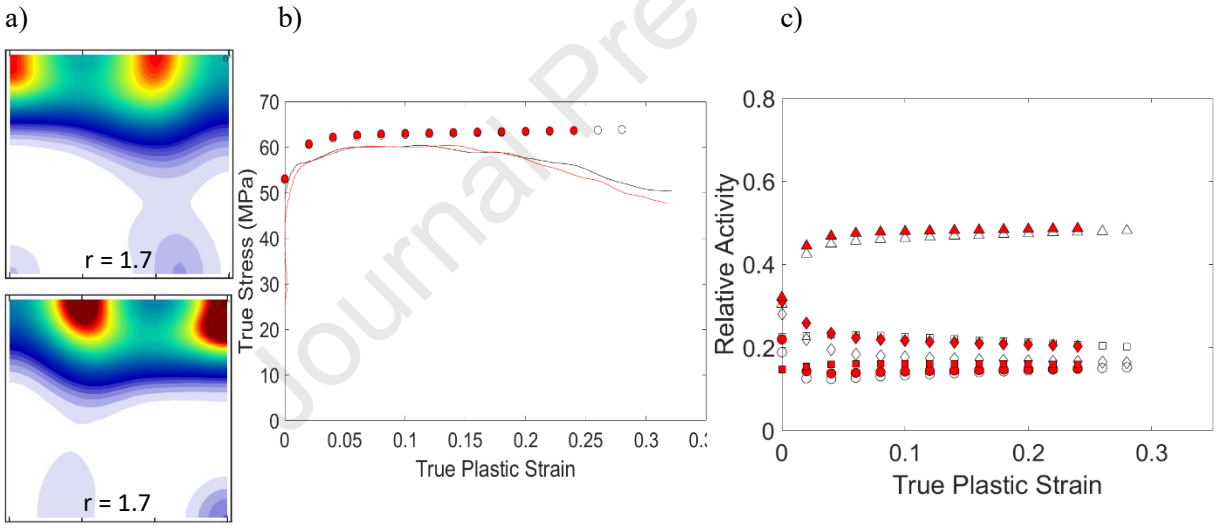

Figure 13: The importance of the character of the climbing dislocations on high temperature simulations (250 °C, 0.001 s^{-1}): a) TD (top) and RD (bottom) textures with associated relative slip activity plots (TD – red, RD – white) using only basal screw dislocation "climb," and c) experimental (TD – red and RD – white) and simulated stress strain curves (circles).

Not surprisingly, modeling of the high temperature response of Mg required the addition of a climb slip mode of deformation. The hypothesis that prism slip is supplanted by <a> climb at high temperatures is supported by a coincident drop in r-value, a dramatic change in the dominant texture component, and a transition to a power-law constitutive regime. What is surprising is the large degree to which climb participates in strain accommodation itself. A sanity check on the requisite climb velocities of these edge dislocations predicted by VPSC-CLIMB is

performed in the discussion section by comparing them with theoretical, diffusion-limited velocities.

5- Discussion

Plausibility of dislocation climb strain accommodation

The Orowan expression links the shear rate of deformation associated with a given mode of climb, $\dot{\gamma}^{c,s}$, to the mobile density of climbing dislocations, ρ_c^s, their Burgers vector, b^s, and their average velocity, $\bar{v}_c^s$.

$$\dot{\gamma}^{c,s} = \rho_c^s b^s \bar{v}_c^s \qquad \text{Equation 14}$$

The fraction of strain accommodated by climb depends on the testing regime (rate and temperature). To check if these VPSC-CLIMB predictions are realistic, the required density of mobile dislocations is computed, based upon a physical model of the steady-state climb velocity. An average value of the shear rate due to climb, $\dot{\gamma}^{c,s}$, was calculated for each of the four high temperature cases we considered in detail, one at 250 °C, 0.001 s^{-1} and three at 350 °C with distinct strain rates, by the summing the shear strain rates of each applicable climb system in each grain of the VPSC-CLIMB simulation. The flow stresses at the relevant conditions were obtained from best-fit Sellars-Tegart model (Equation 13) shown to well-describe the response of the material (Figure 6a).

Since the flow stress is essentially saturated during the test conditions of interest (Figure 5a) one may reasonably assume steady-state motion of the climbing dislocations, i.e., the climb component of the Peach-Koehler force, f_c^s, is balanced by the chemical (drag) force, $f_c^s + f_{chem}^s = 0$. The chemical force was proposed by Bardeen & Herring [61] and Weertman [62] as

$$f_{chem}^s = b\left[\frac{k_B T}{\Omega}\ln\left(\frac{c_v}{c_v^{th}}\right)\right]\mathbf{I}:\boldsymbol{k^s} \qquad \text{Equation 15}$$

$$c_v^{th} = c_v \exp(-p\Omega/k_B T) \qquad \text{Equation 16}$$

where b is the magnitude of the Burgers vector, k_B is Boltzmann's constant, Ω is the volume change due to the formation of a vacancy, c_v is the vacancy concentration at the dislocation core, c_v^{th} is the thermal equilibrium vacancy concentration at a given temperature (T) and *pressure* (p), $\mathbf{I}$ is the identity matrix and $\boldsymbol{k}^s$ is the aforementioned Hartley tensor, $\boldsymbol{k^s}$. It is noted that the dislocation climb velocity can be affected by the hydrostatic stress due to its effect on the background concentration of vacancies, which will in turn affect the chemical (or osmotic) force on a climbing dislocation and can either slow or accelerate dislocation climb. [2]

[2] As a historical note, Lebensohn et al. [19] rationalized an absence of a chemical force (i.e., the vacancy concentration is everywhere at equilibrium with the surrounding pressure), by assuming that vacancy sources and sinks are so close together that the fluctuations in vacancy concentration induced by dislocation climb are removed as quickly as they are created. Later, the chemical force was treated as a sort of backstress on the climbing dislocation, such that the incompressibility condition ($\dot{\varepsilon}_{kk} = 0$) could be explicitly enforced, with 5 constitutive equations relating to the components of the deviatoric stress and strain rate (Equations 8 and 9) and a 6th equation

Given the direct connection between the rate of vacancy creation or annihilation at the dislocation core and climb velocity, diffusion theory thus provides a direct linkage between the applied deviatoric stress and climb velocity, given the temperature dependent vacancy lattice diffusivity (D_v)

$$v_c{}^s = \frac{\Omega}{b}\left\{z_v D_v c_v^{th}\left[\exp\left(\frac{\Omega(\boldsymbol{k}^{d,s}:\boldsymbol{\sigma}')}{k_B T}\right)-1\right]\right\} \qquad \text{Equation 17}$$

where $z_v = 2\pi/\ln(R/b)$ is the vacancy capture efficiency for a dislocation and has been found to be approximately equal to unity in several studies [63–66]. Notably, this equation directly accounts for the aforementioned effect of pressure because it influences the equilibrium vacancy concentrations in the vicinity (at a distance *R*) of climbing dislocations. At the typically small values of $\exp\left(\Omega\left(\boldsymbol{k}^{d,s}:\boldsymbol{\sigma}'\right)/k_B T\right)-1 \approx \Omega\left(\boldsymbol{k}^{d,s}:\boldsymbol{\sigma}'\right)/k_B T$. Hence, Equation 17 implies an essentially linear dependence of the climb velocity on the applied stress. This equation was used to calculate the steady state climb velocities using an effective, scalar value of the Hartley tensor k_{eff} ~ 0.55 selected to account for the stress state, texture, and possible dislocation characters of interest. Note that unlike its glide analogy, the Schmid factor (which has a maximum value of 0.5), the Hartley factor has a maximum value of 1. The diffusivity prefactor was taken from [67] and the vacancy migration and formation energies were taken from [68].

Inserting the obtained velocities into the Orowan expression (Equation 14) yields *mobile* dislocation densities of 7.7 x 10^{12} – 5.3 x 10^{14} 1/m^2 for tests performed at elevated temperatures in this study (Table 2). Given that only the dislocations with an edge component are really subject to climb, this implies a total dislocation density of at least a factor of 2 more, assuming approximately half of the basal dislocations are of edge character. Note further that these estimates were made assuming that the steady state climb rate is controlled by the lattice diffusion (Equation 17) and neglects the likely role of pipe diffusion, especially in cases close to power law breakdown. Regardless, total dislocation densities 4 – 10 times larger than these mobile dislocation density estimates seem plausible.

Table 2: Densities of mobile, climbing <a> dislocations for each elevated temperature condition tested

Temperature (°C)	Rate (s^{-1})	Mobile, Dislocation Density ($1/m^2$)	Flow stress (MPa)	Global Mechanism
250	1x10^{-3}	5.3 x 10^{14}	58.22	LT power law creep
350	1x10^{-1}	1.5 x 10^{14}	57.20	LT/HT creep
350	1x10^{-2}	7.2 x 10^{13}	42.97	HT power law creep
350	2.8x10^{-4}	7.7 x 10^{12}	18.71	GBS

In the present work, which is focused on the kinematics (strain anisotropy and texture evolution), the effect of applied pressure is shown to be of little consequence. By definition, the pressure has an effect on the overall vacancy concentration (Equation 16), but at the given stress and temperature conditions of interest, this leads to an increase in vacancy concentration of less than 10%. Furthermore, this change in vacancy concentration leads to an infinitesimal increase in sample volume which would be recovered upon unloading of the sample. The local fluctuations in vacancy concentration at the dislocation cores are present and what is responsible for the dilatational portion of the Hartley climb tensor. They are accounted for, in the present analysis, by the chemical force (Equation 15). Their effect on the total volume of the sample is again deemed inconsequential for crystal-scale calculations.

Possibility of Grain Boundary Sliding and Other High Temperature Mechanisms

A preliminary method for evaluating the effects of other high temperature mechanisms (grain growth, dynamic recrystallization and GBS) in the current simulation results would be to examine their effects on texture evolution and r-value. Grain growth has two effects on texture evolution in AZ31B: a strengthening of the basal texture [24] and the development of a $< 11\bar{2}0 >$ texture component [25]. It is difficult to identify the source of the basal component strengthening in the experimental textures since it will also occur with the activation of basal slip which is shown to remain active during high temperature deformation. The latter is not experimentally observed in Figures 9 and 10, making its contributions small; additionally, grain growth does not typically accommodate strain and therefore cannot describe the reduction in r-value at high temperatures. Dynamic recrystallization has been shown to cause texture randomization [21,29] and could explain the softening observed in some of the tensile tests performed at high temperatures (Figure 11b). However, it appears that the texture evolution is slowed rather than randomizing during high temperature deformation (Figure 9), suggesting that another mechanism is dominant. The same figure also points out that glide motion is not suppressed as VPSC-CLIMB simulations show that prism <a> slip is responsible for the texture evolution between 10 and 30% strain. Texture randomization is also characteristic of grain boundary sliding, which suggests that it is unlikely to be solely responsible for the transition into the power law regime. Unlike dynamic recrystallization, grain boundary sliding has also been shown to lead to reduced r-values in AZ31B [37] and could be active during high temperature creep, particular at high temperatures and low strain rates (Figure 1).

We have shown that strain accommodation through dislocation climb is plausible from a density standpoint, but it does not rule out the possibility that GBS works in concert with the aforementioned dislocation climb mechanism, but rather emphasizes the importance of dislocation climb during high temperature deformation and suggests that strain accommodations by dynamic recrystallization and GBS processes may be empirically described by accounting for the kinematics of dislocation climb. The nonlinear regression of the Sellars–Tegart expression (Equation 12) yielded an activation energy (Q = 111 kJ/mol) that do not correspond to either self- or solute-diffusion through the lattice, both of which have activation energies closer to 135 kJ/mol [13]. GBS tends to have an activation energy related to grain boundary diffusion (~90 kJ/mol in Mg) with a sufficiently small grain size [69]. Low temperature power law creep is

often associated with pipe diffusion, having a similar activation energy as boundary diffusion. While no single mechanism seems to match the experimentally observed phenomena, it must be noted that some of the tests examined in the present study are near boundaries on the deformation mechanism map (Figure 5b).

A second, more nuanced approach would be to examine if the "non-dislocation" mechanisms of DRX and GBS can be explained by the motion of dislocations and *disconnections* – line defects which are restricted to interfaces such as grain boundaries and have both a Burgers vector and interfacial step height. In general, grain boundaries in metals tend to be curved, which provides an obstacle to simple glide of disconnections. Analogous to dislocations avoiding an impediment (e.g., a precipitate) during deformation, disconnections use a combination of in plane glide and out of plane climb to the move within boundaries during grain growth. MD simulations have shown that grain boundary migration, as in the case of grain growth, is intrinsically linked to the motion of disconnections [70]. In addition, the study suggested that grain boundary sliding can be described as a scenario of grain boundary migration under zero shear stress and non-zero energy density difference between the adjacent grains. A similar mechanism could be used to describe the coupled motion of grain boundaries in Zn bicrystals, as modeled by Cahn et al. [71]. The disconnection climb rate is also important to the possibility of continuous DRX at higher strain rates [72]. As discussed above, the dislocation climb velocity is intrinsically linked to the rate of vacancy diffusion. In short, many of the effects of "non-dislocation" based deformation mechanisms on deformation texture evolution might be attributable to dislocation climb. VPSC-CLIMB simulations were performed on a sample tested within the GBS regime (Figure 5b) as a preliminary test of this theory (Figure 10c). Extremely high climb accommodation (>85% of strain) appears to predict the r-value and slowed texture evolution which occur in this regime, however, there appears to be a mismatch between experimental and simulated textures. Both of the experimental textures have nodes at $\varphi_1 = 0°$ regardless of testing condition, while the simulated textures have nodes at $\varphi_1 = 30°$ (the same orientation as in the initial as-rolled texture) due to suppressed texture evolution from dominant strain accommodation by climb. Here, it is unclear whether this difference is significant due to the near uniformity of the texture, but it warrants further study to elucidate the distinction between climb and grain boundary sliding on texture evolution.

We conclude with a final reflection on previous work [14], in which the most rapid decrease in strain anisotropy was found to occur below the recrystallization temperature (~200 °C) and was attributed to the activation of non-basal slip, following Agnew & Duygulu [3]. The VPSC simulations performed in this study show that the reduction in r-value is not the result of increased non-basal slip, but rather the activation of dislocation climb and accompanied *decrease* in non-basal slip activity. It is emphasized that the activation of dislocation climb explains the reduction in r-value and the increase in rate sensitivity [73] as well as the slowed texture evolution. GBS was offered as a plausible explanation for observations of isotropic flow at lower strain rates [14]. Indeed that is likely, yet many of the effects of such "non-dislocation" based deformation mechanisms on deformation texture evolution are shown to be describable in terms of the kinematics of dislocation climb. So far, the present modeling strategy of incorporating dislocation climb within the matrix appears to best capture the trends in anisotropy and texture

evolution during high temperature deformation of a Mg alloy. Further research is required to integrate and reconcile these findings with concurrent findings related to grain growth, dynamic recrystallization, and in particular, grain boundary sliding [27,74,75] especially at the highest temperatures and lowest strain rates explored.

6- Conclusions

This study was performed to examine the extent to which dislocation climb accommodates strain during the high temperature, in-plane tensile deformation of a model Mg alloy, AZ31B, sheet material. In agreement with previous studies, decreases in anisotropy and slowed texture evolution were experimentally observed to occur simultaneously as the test temperature was raised. The following major conclusions can be drawn:

- VPSC-CLIMB simulations run with parameters best-fit by a genetic algorithm show that the climb of abundant <a> dislocations sustains a significant amount of strain during in-plane tensile deformation of basal textured AZ31B sheet in the power law creep regime.
- VPSC-CLIMB simulations suggest that decreasing the strain rate leads to increased strain accommodation by dislocation climb.
- Densities of climbing dislocations required of each simulated condition were estimated using an Orowan expression based upon the steady-state, lattice diffusion-controlled climb velocity, and they were found to be plausible for every condition ($< 10^{15}$ m^{-2}).
- While a strong increase in <c+a> slip activity can explain the decreased r-values of Mg alloys at moderately elevated temperatures, it cannot simultaneously explain the observed changes in texture evolution, rate sensitivity, and activation energy that attend this transition.
- The enhanced climb of edge dislocations at elevated temperatures can explain the observed changes in constitutive response, in addition to the kinematic elements (texture and strain anisotropy) on which the present work focused.

Author Contributions: M.A. Ritzo – Investigation, Writing – original draft, R.H Lebensohn – Software, Writing – review & editing, L. Capolungo – Visualization, Writing – review & editing, S.R. Agnew – Conceptualization, Supervision, Writing – original draft, Writing – review & editing

Acknowledgements: The researchers at UVA would like to express their gratitude to the United States National Science Foundation, Division of Materials Research, Metals and Metallic Nanostructures (NSF-DMR-MMN) program, Grant No. 1810197, overseen by Dr. Judith Yang. LANL researchers would like to acknowledge BES project E8C5 and XMAT.

Data availability: The raw/processed data required to reproduce these findings cannot be shared at this time due to technical or time limitations.

References

[1] A.K. Ghosh, Tensile instability and necking in materials with strain hardening and strain-rate hardening, Acta Metall. 25 (1977) 1413–1424. https://doi.org/10.1016/0001-6160(77)90072-4.

[2] A. Couret, D. Caillard, An in situ study of prismatic glide in magnesium-I. The rate

controlling mechanism, Acta Metall. 33 (1985) 1447–1454. https://doi.org/10.1016/0001-6160(85)90045-8.

[3] S.R. Agnew, Ö. Duygulu, Plastic anisotropy and the role of non-basal slip in magnesium alloy AZ31B, Int. J. Plast. 21 (2005) 1161–1193. https://doi.org/10.1016/j.ijplas.2004.05.018.

[4] R. V Mises, Mechanik der plastischen Formänderung von Kristallen, ZAMM - J. Appl. Math. Mech. / Zeitschrift Für Angew. Math. Und Mech. 8 (1928) 161–185. https://doi.org/https://doi.org/10.1002/zamm.19280080302.

[5] S.R. Agnew, J.A. Horton, M.H. Yoo, Transmission electron microscopy investigation of ⟨c + a⟩ dislocations in Mg and α-solid solution Mg-Li alloys, Metall. Mater. Trans. A Phys. Metall. Mater. Sci. 33 (2002) 851–858. https://doi.org/10.1007/s11661-002-0154-x.

[6] S.R. Agnew, M.H. Yoo, C.N. Tomé, Application of texture simulation to understanding mechanical behavior of Mg and solid solution alloys containing Li or Y, Acta Mater. 49 (2001) 4277–4289. https://doi.org/10.1016/S1359-6454(01)00297-X.

[7] S. Ando, H. Rikihisa, M. Tsushida, H. Kitahara, Activities of non-basal slips in deformation of magnesium alloy single and poly crystals, Mater. Sci. Forum. 941 MSF (2018) 1242–1247. https://doi.org/10.4028/www.scientific.net/MSF.941.1242.

[8] T. Obara, H. Yoshinga, S. Morozumi, {11$\bar{2}$2}⟨1123⟩ Slip system in magnesium, Acta Metall. 21 (1973) 845–853. https://doi.org/10.1016/0001-6160(73)90141-7.

[9] H. Wang, B. Raeisinia, P.D. Wu, S.R. Agnew, C.N. Tomé, Evaluation of self-consistent polycrystal plasticity models for magnesium alloy AZ31B sheet, Int. J. Solids Struct. 47 (2010) 2905–2917. https://doi.org/10.1016/j.ijsolstr.2010.06.016.

[10] Z. Wu, R. Ahmad, B. Yin, S. Sandlöbes, W.A. Curtin, Mechanistic origin and prediction of enhanced ductility in magnesium alloys, Science (80-.). 359 (2018) 447–452. https://doi.org/10.1017/s0368393100107606.

[11] K. Máthis, K. Nyilas, A. Axt, I. Dragomir-Cernatescu, T. Ungár, P. Lukáč, The evolution of non-basal dislocations as a function of deformation temperature in pure magnesium determined by X-ray diffraction, Acta Mater. 52 (2004) 2889–2894. https://doi.org/10.1016/j.actamat.2004.02.034.

[12] R.A. Lebensohn, C.N. Tomé, A self-consistent anisotropic approach for the simulation of plastic deformation and texture development of polycrystals: Application to zirconium alloys, Acta Metall. Mater. 41 (1993) 2611–2624. https://doi.org/10.1016/0956-7151(93)90130-K.

[13] M.E. Kassner, Fundamentals of Creep in Metals and Alloys, 2nd ed., Butterworth Heinemann, Waltham, MA, 2009.

[14] A.R. Antoniswamy, E.M. Taleff, L.G. Hector, J.T. Carter, Plastic deformation and ductility of magnesium AZ31B-H24 alloy sheet from 22 to 450°C, Mater. Sci. Eng. A. 631 (2015) 1–9. https://doi.org/10.1016/j.msea.2015.02.018.

[15] F.J. Polesak, C.E. Dreyer, T.J. Shultz, S.R. Agnew, Blind study of the effect of processing

history on the constitutive behaviour of alloy AZ31B, Magnes. Technol. (2009) 491–496.

[16] S.S. Vagarali, T.G. Langdon, Deformation mechanisms in h.c.p. metals at elevated temperatures-I. Creep behavior of magnesium, Acta Metall. 29 (1981) 1969–1982. https://doi.org/10.1016/0001-6160(81)90034-1.

[17] S.S. Vagarali, T.G. Langdon, Deformation mechanisms in h.c.p. metals at elevated temperatures-II. Creep behavior of a Mg-0.8% Al solid solution alloy, Acta Metall. 30 (1982) 1157–1170. https://doi.org/10.1016/0001-6160(82)90009-8.

[18] H. Somekawa, K. Hirai, H. Watanabe, Y. Takigawa, K. Higashi, Dislocation creep behavior in Mg-Al-Zn alloys, Mater. Sci. Eng. A. 407 (2005) 53–61. https://doi.org/10.1016/j.msea.2005.06.059.

[19] R.A. Lebensohn, C.S. Hartley, C.N. Tome, O. Castelnau, Modeling the mechanical response of polycrystals deforming by climb and glide, Philos. Mag. 90 (2010) 567–583. https://doi.org/10.1080/14786430903213320.

[20] J. Weertman, Theory of steady-state creep based on dislocation climb, J. Appl. Phys. 26 (1955) 1213–1217. https://doi.org/10.1063/1.1721875.

[21] K.J. Tam, M.W. Vaughan, L. Shen, M. Knezevic, I. Karaman, G. Proust, Modelling dynamic recrystallisation in magnesium alloy AZ31, Int. J. Plast. 142 (2021) 102995. https://doi.org/10.1016/j.ijplas.2021.102995.

[22] K. Zhang, J.R. Weertman, J.A. Eastman, Rapid stress-driven grain coarsening in nanocrystalline Cu at ambient and cryogenic temperatures, Appl. Phys. Lett. 87 (2005) 1–4. https://doi.org/10.1063/1.2008377.

[23] D.S. Gianola, S. Van Petegem, M. Legros, S. Brandstetter, H. Van Swygenhoven, K.J. Hemker, Stress-assisted discontinuous grain growth and its effect on the deformation behavior of nanocrystalline aluminum thin films, Acta Mater. 54 (2006) 2253–2263. https://doi.org/10.1016/j.actamat.2006.01.023.

[24] J.J. Bhattacharyya, S.R. Agnew, G. Muralidharan, Texture enhancement during grain growth of magnesium alloy AZ31B, Acta Mater. 86 (2015) 80–94. https://doi.org/10.1016/j.actamat.2014.12.009.

[25] M.A. Steiner, J.J. Bhattacharyya, S.R. Agnew, The origin and enhancement of {0001} <112¯0> texture during heat treatment of rolled AZ31B magnesium alloys, Acta Mater. 95 (2015) 443–455. https://doi.org/10.1016/j.actamat.2015.04.043.

[26] Y.I. Liu, X.I.N. Wu, 57-Liu-Wu2006_Article_AnElectron-backscatteredDiffra.pdf, 37 (2006) 7–17.

[27] Y. Zhao, L.S. Toth, R. Massion, W. Skrotzki, Role of Grain Boundary Sliding in Texture Evolution for Nanoplasticity, Adv. Eng. Mater. 1700212 (2017) 1–9. https://doi.org/10.1002/adem.201700212.

[28] A. Staroselsky, L. Anand, A constitutive model for hcp materials deforming by slip and twinning: Application to magnesium alloy AZ31B, Int. J. Plast. 19 (2003) 1843–1864. https://doi.org/10.1016/S0749-6419(03)00039-1.

[29] T. Al-Samman, G. Gottstein, Dynamic recrystallization during high temperature deformation of magnesium, Mater. Sci. Eng. A. 490 (2008) 411–420. https://doi.org/10.1016/j.msea.2008.02.004.

[30] H.W. Son, J.W. Lee, S.K. Hyun, Mechanism of grain boundary serration during hot deformation of AZ31 alloy: Role of grain boundary dislocations and grain boundary sliding, Int. J. Plast. 125 (2020) 118–132. https://doi.org/10.1016/j.ijplas.2019.09.003.

[31] H.A. Khater, A. Serra, R.C. Pond, J.P. Hirth, The disconnection mechanism of coupled migration and shear at grain boundaries, Acta Mater. 60 (2012) 2007–2020. https://doi.org/10.1016/j.actamat.2012.01.001.

[32] R. Raj, M.F. Ashby, On grain boundary sliding and diffusional creep, Metall. Trans. 2 (1971) 1113–1127. https://doi.org/10.1007/BF02664244.

[33] O.A. Ruano, J. Wadsworth, O.D. Sherby, Deformation of fine-grained alumina by grain boundary sliding accommodated by slip, Acta Mater. 51 (2003) 3617–3634. https://doi.org/10.1016/S1359-6454(03)00180-0.

[34] A. Ball, M.M. Hutchison, Superplasticity in the Aluminium–Zinc Eutectoid, Met. Sci. J. 3 (1969) 1–7. https://doi.org/10.1179/msc.1969.3.1.1.

[35] R.Z. Valiev, T.G. Langdon, An Investigation of the Role of Intragranular Dislocation Strain in the Superplastic Pb-62% Sn Eutectic Alloy, Acta Met. Mater. 41 (1993) 949–954.

[36] M.F. Ashby, R.A. Verrall, Diffusion-accommodated flow and superplasticity, Acta Metall. 21 (1973) 149–163. https://doi.org/10.1016/0001-6160(73)90057-6.

[37] M.R. Barnett, A. Ghaderi, I. Sabirov, B. Hutchinson, Role of grain boundary sliding in the anisotropy of magnesium alloys, Scr. Mater. 61 (2009) 277–280. https://doi.org/10.1016/j.scriptamat.2009.04.001.

[38] S.R. Agnew, C.N. Tomé, D.W. Brown, T.M. Holden, S.C. Vogel, Study of slip mechanisms in a magnesium alloy by neutron diffraction and modeling, Scr. Mater. 48 (2003) 1003–1008. https://doi.org/10.1016/S1359-6462(02)00591-2.

[39] A. Styczynski, C. Hartig, J. Bohlen, D. Letzig, Cold rolling textures in AZ31 wrought magnesium alloy, Scr. Mater. 50 (2004) 943–947. https://doi.org/10.1016/j.scriptamat.2004.01.010.

[40] M.R. Barnett, Twinning and the ductility of magnesium alloys. Part I: “Tension” twins, Mater. Sci. Eng. A. 464 (2007) 1–7. https://doi.org/10.1016/j.msea.2006.12.037.

[41] A. Jain, S.R. Agnew, Modeling the temperature dependent effect of twinning on the behavior of magnesium alloy AZ31B sheet, Mater. Sci. Eng. A. 462 (2007) 29–36. https://doi.org/10.1016/j.msea.2006.03.160.

[42] L. Jiang, J.J. Jonas, A.A. Luo, A.K. Sachdev, S. Godet, Twinning-induced softening in polycrystalline AM30 Mg alloy at moderate temperatures, Scr. Mater. 54 (2006) 771–775. https://doi.org/10.1016/j.scriptamat.2005.11.029.

[43] J.F. Stohr, J.P. Poirier, Etude en microscopie electronique du glissement pyramidal {1122} ⟨1123⟩ dans le magnesium, Philos. Mag. A J. Theor. Exp. Appl. Phys. 25 (1972) 1313–1329. https://doi.org/10.1080/14786437208223856.

[44] G. Edelin, J.P. Poirier, Etude de la montée des dislocations au moyen d'expériences de fluage par diffusion dans le magnésium, Philos. Mag. A J. Theor. Exp. Appl. Phys. 28 (1973) 1211–1223. https://doi.org/10.1080/14786437308227995.

[45] F.K. Abu-Farha, M.K. Khraisheh, Analysis of superplastic deformation of AZ31 magnesium alloy, Adv. Eng. Mater. 9 (2007) 777–783. https://doi.org/10.1002/adem.200700155.

[46] H.J. Frost, M.F. Ashby, Deformation-mechanism Maps: The Plasticity and Creep of Metals and Ceramics, Elsevier Science Limited, 1982. https://books.google.com/books?id=5PpDAQAAIAAJ.

[47] F. Bachmann, R. Hielscher, H. Schaeben, Texture analysis with MTEX- Free and open source software toolbox, Solid State Phenom. 160 (2010) 63–68. https://doi.org/10.4028/www.scientific.net/SSP.160.63.

[48] H.R.W. U.F. Kocks, C. N. Tome, Texture And Anisotropy:Preferred Orientations in Polycrystals and Theire Effect on Materials Properties, (1998) 1–676.

[49] V. Randle, O. Engler, Introduction to Texture Analysis, 2000. https://doi.org/10.1016/j.dss.2003.08.004.

[50] C.S. Hartley†, A method for linking thermally activated dislocation mechanisms of yielding with continuum plasticity theory, Philos. Mag. 83 (2003) 3783–3808. https://doi.org/10.1080/14786430310001599522.

[51] U.F. Kocks, H. Mecking, Physics and phenomenology of strain hardening: The FCC case, Prog. Mater. Sci. 48 (2003) 171–273. https://doi.org/10.1016/S0079-6425(02)00003-8.

[52] C.N. Tomé, R.A. Lebensohn, Manual for Code Version 7b (last updated : May 2 , 2007), (2007).

[53] I.J. Beyerlein, C.N. Tomé, A dislocation-based constitutive law for pure Zr including temperature effects, Int. J. Plast. 24 (2008) 867–895. https://doi.org/10.1016/j.ijplas.2007.07.017.

[54] R.A. Lebensohn, R.A. Holt, A. Caro, A. Alankar, C.N. Tomé, Improved constitutive description of single crystal viscoplastic deformation by dislocation climb, Comptes Rendus - Mec. 340 (2012) 289–295. https://doi.org/10.1016/j.crme.2012.02.011.

[55] T. Skippon, C. Mareau, M.R. Daymond, On the determination of single-crystal plasticity parameters by diffraction: optimization of a polycrystalline plasticity model using a genetic algorithm, J. Appl. Crystallogr. 45 (2012) 627–643. https://doi.org/10.1107/S0021889812026854.

[56] D.J. Savage, Z. Feng, M. Knezevic, Identification of crystal plasticity model parameters by multi-objective optimization integrating microstructural evolution and mechanical data, Comput. Methods Appl. Mech. Eng. 379 (2021) 113747.

https://doi.org/https://doi.org/10.1016/j.cma.2021.113747.

[57] T. Ebeling, C. Hartig, T. Laser, R. Bormann, Material law parameter determination of magnesium alloys, Mater. Sci. Eng. A. 527 (2009) 272–280. https://doi.org/10.1016/j.msea.2009.07.072.

[58] C.M. Sellars, W.J.M. Tegart, Hot Workability, Int. Metall. Rev. 17 (1972) 1–24. https://doi.org/10.1179/imtlr.1972.17.1.1.

[59] E. Calvert, J. Pollard, M. Jackson, B. Wynne, R. Thackray, Determining a flow stress model for high temperature deformation of Ti-6Al-4V, Mater. Sci. Forum. 828–829 (2015) 441–446. https://doi.org/10.4028/www.scientific.net/MSF.828-829.441.

[60] W. Blum, P. Eisenlohr, Dislocation mechanics of creep, Mater. Sci. Eng. A. 510–511 (2009) 7–13. https://doi.org/10.1016/j.msea.2008.04.110.

[61] J. Bardeen, C. Herring, Imperfections in Nearly Perfect Crystals, Wiley, New York, 1952.

[62] J. Weertman, The Peach–Koehler equation for the force on a dislocation modified for hydrostatic pressure, Philos. Mag. A J. Theor. Exp. Appl. Phys. 11 (1965) 1217–1223. https://doi.org/10.1080/14786436508224930.

[63] Z. Chang, D. Terentyev, N. Sandberg, K. Samuelsson, P. Olsson, Anomalous bias factors of dislocations in bcc iron, J. Nucl. Mater. 461 (2015) 221–229. https://doi.org/10.1016/j.jnucmat.2015.03.025.

[64] K.M. Davoudi, L. Nicola, J.J. Vlassak, Dislocation climb in two-dimensional discrete dislocation dynamics, J. Appl. Phys. 111 (2012). https://doi.org/10.1063/1.4718432.

[65] M. Huang, Z. Li, J. Tong, The influence of dislocation climb on the mechanical behavior of polycrystals and grain size effect at elevated temperature, Int. J. Plast. 61 (2014) 112–127. https://doi.org/10.1016/j.ijplas.2014.06.002.

[66] W. Wen, A. Kohnert, M. Arul Kumar, L. Capolungo, C.N. Tomé, Mechanism-based modeling of thermal and irradiation creep behavior: An application to ferritic/martensitic HT9 steel, Int. J. Plast. 126 (2020). https://doi.org/10.1016/j.ijplas.2019.11.012.

[67] P.G. Shewmon, F.N. Rhines, Rate of Self-Diffusion in Polycrystalline Magnesium, JOM. 6 (1954) 1021–1025. https://doi.org/10.1007/BF03398339.

[68] B.C. Zhou, S.L. Shang, Y. Wang, Z.K. Liu, Diffusion coefficients of alloying elements in dilute Mg alloys: A comprehensive first-principles study, Acta Mater. 103 (2016) 573–586. https://doi.org/10.1016/j.actamat.2015.10.010.

[69] T.G. Langdon, Grain boundary sliding revisited: Developments in sliding over four decades, J. Mater. Sci. 41 (2006) 597–609. https://doi.org/10.1007/s10853-006-6476-0.

[70] S.L. Thomas, K. Chen, J. Han, P.K. Purohit, D.J. Srolovitz, Reconciling grain growth and shear-coupled grain boundary migration, Nat. Commun. 8 (2017) 1–12. https://doi.org/10.1038/s41467-017-01889-3.

[71] J.W. Cahn, Y. Mishin, A. Suzuki, Coupling grain boundary motion to shear deformation, Acta Mater. 54 (2006) 4953–4975. https://doi.org/10.1016/j.actamat.2006.08.004.

[72] Z.Y. Liu, T.T. Huang, W.J. Liu, S. Kang, Dislocation mechanism for dynamic recrystallization in twin-roll casting Mg-5.51Zn-0.49Zr magnesium alloy during hot compression at different strain rates, Trans. Nonferrous Met. Soc. China (English Ed. 26 (2016) 378–389. https://doi.org/10.1016/S1003-6326(16)64126-2.

[73] S.M. Zhu, B.L. Mordike, J.F. Nie, Creep and rupture properties of a squeeze-cast Mg-Al-Ca alloy, Metall. Mater. Trans. A Phys. Metall. Mater. Sci. 37 (2006) 1221–1229. https://doi.org/10.1007/s11661-006-1073-z.

[74] A. Venkataraman, M.D. Sangid, A crystal plasticity model with an atomistically informed description of grain boundary sliding for improved predictions of deformation fields, Comput. Mater. Sci. 197 (2021) 110589. https://doi.org/10.1016/j.commatsci.2021.110589.

[75] A. Venkataraman, M. Linne, S. Daly, M.D. Sangid, Criteria for the prevalence of grain boundary sliding as a deformation mechanism, Materialia. 8 (2019) 100499. https://doi.org/10.1016/j.mtla.2019.100499.

[76] M. Knezevic, M. Zecevic, I.J. Beyerlein, R.A. Lebensohn, A numerical procedure enabling accurate descriptions of strain rate-sensitive flow of polycrystals within crystal visco-plasticity theory, Comput. Methods Appl. Mech. Eng. 308 (2016) 468–482. https://doi.org/10.1016/j.cma.2016.05.025.

[77] W.G. Feather, D.J. Savage, M. Knezevic, A crystal plasticity finite element model embedding strain-rate sensitivities inherent to deformation mechanisms: Application to alloy AZ31, Int. J. Plast. 143 (2021) 103031. https://doi.org/10.1016/j.ijplas.2021.103031.

[78] Y. Gao, A.C.F. Cocks, Thermodynamic Variational Approach for Climb of an Edge Dislocation, Acta Mech. Solida Sin. 22 (2009) 426–435. https://doi.org/10.1016/S0894-9166(09)60293-7.

[79] S.M. Keralavarma, T. Cagin, A. Arsenlis, A.A. Benzerga, Power-law creep from discrete dislocation dynamics, Phys. Rev. Lett. 109 (2012) 1–5. https://doi.org/10.1103/PhysRevLett.109.265504.

[80] C. Ayas, J.A.W. Van Dommelen, V.S. Deshpande, Climb-enabled discrete dislocation plasticity, J. Mech. Phys. Solids. 62 (2014) 113–136. https://doi.org/10.1016/j.jmps.2013.09.019.

[81] S.M. Keralavarma, A.A. Benzerga, High-temperature discrete dislocation plasticity, J. Mech. Phys. Solids. 82 (2015) 1–22. https://doi.org/10.1016/j.jmps.2015.05.003.

[82] P.A. Geslin, B. Appolaire, A. Finel, Multiscale Theory of Dislocation Climb, Phys. Rev. Lett. 115 (2015) 1–5. https://doi.org/10.1103/PhysRevLett.115.265501.

- <c+a> slip cannot explain the texture evolution during high temperature testing.
- VPSC modeling of Mg alloy sheet deformation required significant dislocation climb.
- Machine learning can assist in fitting experimental textures and r-values.

Declaration of interests

☒The authors declare that they have no known competing financial interests or personal relationships that could have appeared to influence the work reported in this paper.

☐The authors declare the following financial interests/personal relationships which may be considered as potential competing interests: